On the critical solutions in coating and rimming flow on a uniformly rotating horizontal cylinder

S. K. Wilson,* R. Hunt† and B. R. Duffy‡

Department of Mathematics,

University of Strathclyde,

Livingstone Tower,

26 Richmond Street,

Glasgow G1 1XH,

United Kingdom

11th May 2001, revised 3rd September 2001

*Email : s.k.wilson@strath.ac.uk, Telephone : + 44 (0) 141 548 3820, Fax : + 44 (0) 141 552 8657

†Email : r.hunt@strath.ac.uk, Telephone : + 44 (0) 141 548 3658, Fax : + 44 (0) 141 552 8657

‡Email : b.r.duffy@strath.ac.uk, Telephone : + 44 (0) 141 548 3645, Fax : + 44 (0) 141 552 8657

Abstract

We use a combination of analytical and numerical techniques to re-examine the question posed by Moffatt [*J. Méc.* **16** (1977) 651–673] of determining the critical weights of fluid that can be maintained per unit length in a steady, smoothly varying, two-dimensional film on either the outside ("coating flow") or the inside ("rimming flow") of a rotating horizontal cylinder. We use a pseudospectral method to obtain highly accurate numerical solutions for steady Stokes flow on a cylinder and hence to calculate the critical weights. In particular, these calculations reveal that the behaviour of the critical solutions in the thin-film limit $\delta \to 0$ (where δ is the aspect ratio of the film) in an inner region near the horizontal on the ascending side of the cylinder (where Moffatt's leading-order outer solution has a corner) are not captured by naive outer asymptotic solutions in integer powers of δ. Motivated by these numerical results we obtain the uniformly valid critical asymptotic solutions in the thin-film limit to sufficient accuracy to enable us to calculate the critical fluxes and weights to accuracies $o(\delta^{4/3}(\log\delta)^{-3})$ and $o(\delta^{4/3}(\log\delta)^{-2})$ relative to Moffatt's leading-order values, respectively. We find that our asymptotic solutions for the critical weights are in good agreement with the numerically calculated results over a wide range of values of δ. In particular, our numerical and asymptotic calculations show that, even in the absence of surface-tension effects, the corner predicted by Moffatt's leading-order outer solution never actually occurs. In practice the higher-order terms obtained in the present work dominate the formally lower-order term that can be obtained straightforwardly without a detailed knowledge of the solution in the inner region, and so these higher-order terms must be included in order to obtain accurate corrections to Moffatt's leading-order value of the critical weight. In particular, in practice the critical weights in both coating and rimming flow always exceed Moffatt's value.

1 Introduction

This paper revisits the fascinating question posed by Moffatt [1] of determining the critical weights of Newtonian fluid of uniform density ρ and kinematic viscosity ν that can be maintained per unit length in a steady, smoothly varying, two-dimensional film on either the outside or the inside of a horizontal circular cylinder of radius a rotating anti-clockwise at a constant angular speed ω, as a result of a balance between viscous and gravitational forces. As well as being an important fundamental theoretical question concerning viscous flows with a free surface, it is also of relevance to a number of practical situations including several industrial coating processes.

In flow on the outside of a cylinder (usually called "coating flow") load shedding occurs when the weight of fluid is increased above its critical value. In flow on the inside of a cylinder (usually called "rimming flow") all the fluid is contained within the cylinder and so load shedding is, of course, impossible, and increasing the weight slightly above its critical value has the rather less dramatic effect of causing the film thickness to develop a region of rapid variation as the excess fluid accumulates in the lower part of the cylinder. Experimental investigations of the interesting unsteady and three-dimensional flows that can develop in both coating and rimming situations have been undertaken by, for example, Balmer [2], Karweit & Corrsin [3], Balmer & Wang [4], Moffatt [1], Kovac & Balmer [5], Joseph & Preziosi [6], Preziosi & Joseph [7], Melo [8], Melo & Douady [9], Vallette, Edwards & Gollub [10], Thoroddsen & Mahadevan [11, 12], Vallette, Jacobs & Gollub [13], and Boote & Thomas [14].

In his pioneering paper Moffatt [1] gave the steady two-dimensional leading-order solution for both coating and rimming flow in the asymptotic limit in which the aspect ratio of the film, defined by

$$\delta = \left(\frac{\nu\omega}{ga}\right)^{1/2} \tag{1}$$

(where g denotes acceleration due to gravity) approaches zero, that is, in which the film is thin. Moffatt showed that this solution (in which both inertia and surface-tension

effects are neglected) has a critical non-dimensional weight per unit axial length of 4.44272 which occurs at a maximum non-dimensional azimuthal volume flux per unit axial length of two thirds. This critical solution has the rather unusual property that the free surface has a corner at $\theta = 0$ (where θ is the azimuthal coordinate measured anti-clockwise from the horizontal on the ascending side of the cylinder) near which the non-dimensional thickness of the fluid film is given by $1 - |\theta|/\sqrt{6} + O(\theta^2)$.[1] The critical film thickness has a maximum value of unity at $\theta = 0$ and a minimum value of 0.5961 at $\theta = \pi$. Aspects of Moffatt's analysis are contained in the earlier work by Van Rossum [16] on the classical "drag out" problem. The corresponding leading-order solution for thin-film flow of a viscoplastic material (modelled as a biviscosity fluid with a yield stress) was recently obtained by Ross, Wilson & Duffy [17].

Moffatt's analysis was extended by Duffy & Wilson [15] to include solutions that are unbounded at $\theta = \pm\frac{1}{2}\pi$ (where the lubrication approximation therefore fails). These "curtain" solutions are physically sensible only in coating flow, where they provide a crude model for a curtain of fluid falling onto and off the cylinder; they can be regarded as generalisations of the classical solution of Nusselt [18, 19] for curtain flow round a stationary cylinder. Unlike Moffatt's solution, curtain solutions are possible for all values of the weight and so the question of a critical weight does not arise in this case.

By considering the first-order correction in the aspect ratio δ to Moffatt's leading-order solution Johnson [20] showed how in rimming flow (but *not* in coating flow), Moffatt's solution can be extended to include solutions with one or two regions of rapid variation in thickness, both with and without dry patches (termed "partial-film" and "jump" solutions respectively by Duffy & Wilson [15]) whose weight can exceed the critical value for smooth solutions. By extending the analysis of Johnson [20], Duffy & Wilson [15] showed that, in contrast to Moffatt's solution, curtain solutions allow the

[1] As Duffy & Wilson [15] pointed out, Moffatt gave a slightly inaccurate value of 4.428 (instead of 4.44272) for the numerical coefficient in his expression for the critical weight in his equation (25), and an incorrect value of 0.866 (instead of $\sqrt{6}/4 \approx 0.612$) for the coefficient of $|\theta|$ in his expression for the film thickness in the footnote on his page 658.

possibility of both partial-film and jump solutions in coating flow.

As we have already mentioned, in rimming flow when the weight slightly exceeds its critical value of 4.44272 the film thickness develops a region of rapid variation in the quadrant between $\theta = -\frac{1}{2}\pi$ and $\theta = 0$. As Johnson [20], O'Brien & Gath [21] and Tirumkudulu & Acrivos [22] describe, the leading-order thin-film solution can be used to model this behaviour as a "shock" solution that has a discontinuity in film thickness and, in particular, to predict the location and height of the shock. This solution predicts a region of backflow (absent in Moffatt's solution) when the non-dimensional weight exceeds 4.98229, but fails when it reaches 6.92607.[2] Tirumkudulu & Acrivos [22] proposed an extension to Moffatt's leading-order solution that selectively retains certain first-order terms in δ due to the hydrostatic pressure, and found excellent agreement between their predictions for the film thickness and both numerical solutions of the full Stokes equations and experimental results for several supercritical values of the weight. Taking a slightly different approach Wilson & Williams [23] numerically solved an evolution equation for rimming flow that incorporates the smoothing effect of surface tension, and they found that for the particular case they considered with a slightly supercritical value of the weight, a steady solution eventually develops with a single region of rapid variation whose location is in good agreement with the prediction of the leading-order thin-film solution. Hosoi & Mahadevan [24] numerically solved an evolution equation for rimming flow incorporating both weak surface-tension and weak inertia effects and obtained both steady and unsteady two-dimensional solutions. They also calculated steady three-dimensional flows resembling the "shark-teeth" pattern observed experimentally. The linear stability of steady two-dimensional rimming flow has been investigated by Johnson [25] and more recently by Hosoi & Mahadevan [24], who found that it is linearly stable to axial perturbations when inertia effects are weak but linearly unstable when inertia effects are sufficiently strong.

[2]Note that the corresponding critical values given by Tirumkudulu & Acrivos [22], namely 1.5862 and 2.2135, are slightly inaccurate and should be 1.5859 and 2.2046.

Complementing the above analytical work on thin-film flows are numerical studies of situations when the film is not thin. Hansen & Kelmanson [26] used an integral-equation method to compute steady coating-flow solutions to the full Stokes equations for several values of δ between 0.2 and 1. In particular, they found that for all the parameter values they investigated the critical film is always thickest at $\theta = 0$ and thinnest at $\theta = \pi$ (as it is in Moffatt's solution) and that the numerically calculated critical weight lies close to, but always somewhat above, Moffatt's value, the difference diminishing as δ is decreased. Interestingly, even for the smallest value of δ they considered ($\delta = 0.2$), their numerically calculated critical film thicknesses show no hint of the corner at $\theta = 0$ present in Moffatt's leading-order solution; as we shall show subsequently this observation is consistent with our own numerical and asymptotic results. Most of Hansen & Kelmanson's [26] numerical calculations are (like Moffatt's solution) for the case of zero surface tension, but they also undertook some calculations including surface tension and concluded that significant variations from their earlier results occur only for unphysically large values of the surface tension. More recently, Peterson, Jimack & Kelmanson [27] used a mixed finite-element method applied on a continuously deforming grid to compute unsteady coating-flow solutions to the full Stokes equations for a range of values of δ. The results of these calculations broadly confirm the values of critical weight obtained by earlier authors and show, rather unexpectedly, that steady states are more readily attained for near-critical weights. Their calculations for supercritical values of the weight show dramatic evidence of load shedding.

Kelmanson [28] proposed an extension to Moffatt's leading-order solution that selectively retains some, but not all, of the first-order terms in δ. In particular, for coating flow this approach yields a positive correction to Moffatt's leading-order value of the critical weight that results in improved agreement with Hansen & Kelmanson's [26] numerical results. However, as the present work shows, if *all* of the first-order terms are included then the true correction is in fact *negative* and so makes the agreement worse! The numerical and asymptotic results in the present work show that in order to obtain

improved agreement it is necessary to include corrections that formally are of higher order but which in practice dominate the first-order correction for all but unphysically small values of δ.

The first experimental investigation of the critical conditions in both coating and rimming flows was apparently undertaken by Preziosi & Joseph [7] who found good agreement with a local "run-off" condition equivalent to the requirement that the volume flux takes its maximum value in Moffatt's leading-order solution despite the fact that the films were not two-dimensional but had significant variations in the axial direction. Subsequently, Kelmanson [28] reported measurements of the critical weight from a simple coating-flow experiment for several values of δ between approximately 0.06 and 0.23 which are in reasonable agreement with his approximate theory. Kelmanson [28] did not show a comparison with Moffatt's leading-order value for the critical weight; we shall show subsequently that Kelmanson's [28] experimental values of the critical weight lie reasonably close to, but definitely below, Moffatt's value.

In the present paper we use a combination of analytical and numerical techniques to re-examine the question posed by Moffatt of determining the critical weights of fluid that can be maintained per unit length in a steady, smoothly varying, two-dimensional film in either coating or rimming flow on a rotating horizontal cylinder. In §2 the appropriate mathematical problem is formulated. In §3 we use a pseudospectral method to obtain highly accurate numerical solutions for steady Stokes flow and hence to calculate the critical weights. In particular, these numerical calculations reveal that the behaviour of the critical solutions in the thin-film limit $\delta \to 0$ in an inner region near $\theta = 0$ (where Moffatt's leading-order outer solution has a corner) are not captured by naive outer asymptotic solutions in integer powers of δ. Motivated by these numerical results we obtain in §4 the uniformly valid critical asymptotic solutions in the thin-film limit to sufficient accuracy to enable us to calculate the critical fluxes and weights to accuracies $o(\delta^{4/3}(\log\delta)^{-3})$ and $o(\delta^{4/3}(\log\delta)^{-2})$ relative to Moffatt's leading-order values, respectively. In §5 we compare our numerical and asymptotic results with each other

and with Hansen & Kelmanson's [26] numerical results, Kelmanson's [28] approximate theory, and Kelmanson's [28] experimental results. Finally in §6 conclusions are drawn.

2 Governing equations and boundary conditions

We consider the steady two-dimensional Stokes flow of a layer of Newtonian fluid of uniform density ρ and viscosity μ on either the exterior ("coating flow") or the interior ("rimming flow") of a circular cylinder of radius a rotating about its horizontal axis at uniform angular speed ω (so that the circumferential speed is $U = a\omega$). The geometry is shown in figure 1 in the case of coating flow; the corresponding geometry for rimming flow can be readily deduced. We refer the description to polar coordinates r, θ with origin at the cylinder's axis and with θ measured anti-clockwise from the horizontal on the ascending side of the cylinder. We denote the thickness of the layer by $h(\theta)$ (so that the free surface of the fluid is at $r = a + h$ for coating flow and $r = a - h$ for rimming flow), the fluid velocity by $\mathbf{u}(r,\theta) = v(r,\theta)\mathbf{e}_r + u(r,\theta)\mathbf{e}_\theta$, where $\mathbf{e}_r$ and $\mathbf{e}_\theta$ denote the unit vectors in the radial and azimuthal directions respectively, and the fluid pressure by $p(r,\theta)$. The unit tangent in the direction of increasing θ and the unit outward normal to the free surface are denoted by $\mathbf{t}$ and $\mathbf{n}$ respectively. The governing equations are the familiar mass conservation and Stokes equations which are to be solved subject to the usual boundary conditions of continuity of velocity at the cylinder together with continuity of stress and the kinematic condition at the free surface. Surface-tension effects are neglected. The conditions for the neglect of inertia and surface tension will be made explicit subsequently.

Moffatt [1] obtained the leading-order solution to this problem in the limit in which the aspect ratio of the layer, given by

$$\delta = \left(\frac{\mu U}{\rho g a^2}\right)^{1/2} = \left(\frac{\nu\omega}{ga}\right)^{1/2}, \tag{2}$$

approaches zero, that is, in which the layer is thin. Since we wish to extend this solution to higher orders it is convenient to non-dimensionalise the problem using a as the

azimuthal length scale, δa as the radial length scale, U as the azimuthal velocity scale, δU as the radial velocity scale, and $\delta\rho ga$ as the pressure scale. Hereafter all quantities will be dimensionless unless stated otherwise.

For coating flow we write $r = 1 + \delta y$; then the governing equations become

$$\frac{\partial v}{\partial y} + \frac{\delta v}{r} + \frac{1}{r}\frac{\partial u}{\partial \theta} = 0, \tag{3}$$

$$0 = -\frac{\partial p}{\partial y} + \delta\left[D^2 v - \frac{2\delta}{r^2}\frac{\partial u}{\partial \theta} - \frac{\delta^2 v}{r^2}\right] - \sin\theta, \tag{4}$$

$$0 = -\frac{\delta}{r}\frac{\partial p}{\partial \theta} + D^2 u + \frac{2\delta^3}{r^2}\frac{\partial v}{\partial \theta} - \frac{\delta^2 u}{r^2} - \cos\theta, \tag{5}$$

where we have written

$$D^2 = \frac{\partial^2}{\partial y^2} + \frac{\delta}{r}\frac{\partial}{\partial y} + \frac{\delta^2}{r^2}\frac{\partial^2}{\partial \theta^2}, \tag{6}$$

the continuity of velocity condition at the cylinder becomes

$$u = 1, \quad v = 0 \quad \text{on} \quad y = 0, \tag{7}$$

and continuity of normal and tangential stress and the kinematic condition at the free surface become

$$p = 2(e_{rr}\cos 2\alpha + e_{r\theta}\sin 2\alpha), \tag{8}$$

$$e_{rr}\sin 2\alpha - e_{r\theta}\cos 2\alpha = 0, \tag{9}$$

$$\delta v\cos\alpha + u\sin\alpha = 0 \tag{10}$$

on $y = h$, where

$$e_{rr} = \delta\frac{\partial v}{\partial y}, \quad e_{r\theta} = \frac{1}{2}\left[\frac{\partial u}{\partial y} - \frac{\delta u}{r} + \frac{\delta^2}{r}\frac{\partial v}{\partial \theta}\right] \tag{11}$$

are components of the rate-of-strain tensor, $\mathbf{n} = (\cos\alpha, \sin\alpha)$, $\mathbf{t} = (-\sin\alpha, \cos\alpha)$, and the angle α (shown in figure 1) is given by

$$\tan\alpha = -\frac{\delta h'}{1 + \delta h} \tag{12}$$

(where a prime denotes $\mathrm{d}/\mathrm{d}\theta$). The flux Q of fluid per unit axial length crossing a station $\theta =$ constant in the direction of increasing θ (made non-dimensional with δaU) is given

by

$$Q = \int_0^h u \, \mathrm{d}y, \tag{13}$$

in terms of which the kinematic condition (10) can (at least for the steady continuous solutions that we shall be concerned with in the present work) be replaced by the simpler statement that Q is a constant. The weight W of fluid on the cylinder per unit axial length (made non-dimensional with $\delta\rho g a^2$) is given by

$$W = \int_0^{2\pi} h + \tfrac{1}{2}\delta h^2 \, \mathrm{d}\theta. \tag{14}$$

For rimming flow we write $r = 1 - \delta y$; we then find that the relevant equations and boundary conditions are identical to those obtained by replacing p with $-p$ and δ by $-\delta$ in those for coating flow given above.

3 Numerical procedure

3.1 Stream-function formulation

In order to solve the present problem numerically it is convenient to reformulate it in terms of a stream function ψ defined by $u = \partial\psi/\partial y$ and $v = -r^{-1}\partial\psi/\partial\theta$. With this choice the continuity equation (3) is satisfied automatically, and (4) and (5) become

$$0 = -\frac{\partial p}{\partial y} - \frac{\delta}{r}\frac{\partial}{\partial\theta}D^2\psi - \sin\theta, \tag{15}$$

$$0 = -\frac{\delta}{r}\frac{\partial p}{\partial\theta} + \frac{\partial}{\partial y}D^2\psi - \cos\theta. \tag{16}$$

Eliminating p between (15) and (16) shows that ψ satisfies the biharmonic equation

$$D^4\psi = 0. \tag{17}$$

The continuity of velocity condition (7) can be written as

$$\psi = 0 \quad \text{and} \quad \frac{\partial\psi}{\partial y} = 1 \quad \text{on} \quad y = 0, \tag{18}$$

and the kinematic condition (10) as

$$\psi = Q \quad \text{on} \quad y = h. \tag{19}$$

We can eliminate p from the normal-stress boundary condition (8) by differentiating along the free surface. Specifically, since

$$\frac{\partial}{\partial n} = \cos\alpha \frac{\partial}{\partial y} + \frac{\delta \sin\alpha}{r} \frac{\partial}{\partial \theta}, \qquad \frac{\partial}{\partial t} = -\sin\alpha \frac{\partial}{\partial y} + \frac{\delta \cos\alpha}{r} \frac{\partial}{\partial \theta},$$

where n and t denote coordinates in the directions of $\mathbf{n}$ and $\mathbf{t}$ respectively, from (15) and (16) we have

$$\frac{\partial p}{\partial t} = \frac{\partial}{\partial n} D^2\psi - \cos(\theta + \alpha),$$

and so (8) can be written as

$$\frac{\partial}{\partial n} D^2\psi - \cos(\theta + \alpha) - 2\frac{\partial}{\partial t}\left(e_{rr} \cos 2\alpha + e_{r\theta} \sin 2\alpha\right) = 0 \quad \text{on} \quad y = h. \tag{20}$$

We therefore solve the biharmonic equation (17) subject to the boundary conditions (9), (18), (19) and (20) for ψ. The unknown value of the flux Q given by (13) is determined by prescribing the weight W of fluid on the cylinder given by (14).

3.2 Transformation and pseudospectral discretisation

The numerical method employed in the present work involves replacing derivatives with pseudospectral differences after the fluid domain $0 \leq y \leq h(\theta)$, $0 \leq \theta \leq 2\pi$ has been transformed onto a rectangular domain in (η, ξ) space by writing $y = H(\xi)\eta$ and $\theta = f(\xi)$, where $H(\xi) = h(f(\xi))$ and $f(0) = 0$, so that

$$\frac{\partial}{\partial y} = \frac{1}{H} \frac{\partial}{\partial \eta}, \qquad \frac{\partial}{\partial \theta} = \frac{1}{f'} \left(\frac{\partial}{\partial \xi} - \frac{H'\eta}{H} \frac{\partial}{\partial \eta} \right). \tag{21}$$

The strictly monotonically increasing function $f(\xi)$ may be chosen so as to cluster the numerical grid points in the θ direction. If this is not necessary then we simply use the uniform grid obtained by setting $f(\xi) = \xi$. However, the numerical calculations reveal that in the critical case there is a region of rapid variation on a length scale of

$O(\delta^{2/3})$ near $\theta = 0$ (see §3.3 for further details of this region), and so in order to resolve the critical solution over several grid points a non-trivial choice of $f(\xi)$ is required. Specifically, we choose $f(\xi)$ so that

$$f'(\xi) = 1 - (1 - c)\tanh(k\cos\xi), \tag{22}$$

where the parameters c and k are at our disposal. If we choose k to be sufficiently large then (22) has $\mathrm{d}\theta/\mathrm{d}\xi = f'(\xi) \approx c$ near $\theta = 0$ and so choosing c to be sufficiently small clusters the grid points near $\theta = 0$. Since the width of the region of rapid variation is $O(\delta^{2/3})$ we choose $c = \delta^{2/3} \ll 1$, and after numerical experimentation it was found that choosing $k = -\log\delta/3$ ensures that it contains sufficient grid points.

A numerical grid of size $m \times n$ is placed on the rectangular domain in (η, ξ) space using the Chebyshev-Gauss-Lobatto points in the η direction scaled onto $0 \leq \eta \leq 1$, and uniform spacing in the ξ direction. All derivatives are then approximated to spectral accuracy using Chebyshev and Fourier collocation differentiation matrices to give a system of nonlinear algebraic equations. There are $N = n(m + 2)$ unknowns, consisting of ψ_{ij}, $i = 0, 1, \ldots, m$, $j = 1, 2, \ldots, n$, and H_j, $j = 1, 2, \ldots, n$, where ψ_{ij} denotes the approximation to ψ at the grid point (η_i, ξ_j) and H_j the approximation to H at ξ_j. The discretised form of (17) is applied at points $i = 2, 3, \ldots, m-2$, $j = 1, 2, \ldots, n$, (18) is applied at $i = 0$, $j = 1, 2, \ldots, n$, and (9) and (20) at $i = m$, $j = 1, 2, \ldots, n$ to give $n(m + 1)$ equations. The flux Q in (19) is unknown and hence we use

$$\psi_{mj} = \psi_{mj+1}, \qquad j = 1, 2, \ldots, n - 1,$$

giving a further $n - 1$ equations. The final equation is given by (14) for a specified weight W. For periodic functions integrated over a full period the trapezoidal rule has spectral accuracy, and so this is used to approximate (14). The system of N equations, of the form $\mathbf{F}(\mathbf{U}) = \mathbf{0}$, where $\mathbf{F}$ and $\mathbf{U}$ are vectors of length N, with $\mathbf{U}$ containing the unknowns, is solved by Newton's method, in which the elements of the Jacobian matrix J are calculated numerically using

$$J_{ij} = \frac{\partial F_i}{\partial U_j} = \frac{1}{2\Delta}\left[\mathbf{F}(U_1, \ldots, U_j + \Delta, \ldots, U_N) - \mathbf{F}(U_1, \ldots, U_j - \Delta, \ldots, U_N)\right],$$

where $\Delta \ll 1$ is set to 10^{-6}.

The accuracy of the calculations can be ascertained by varying m and n separately and comparing the results. As expected, the results exhibit pseudospectral accuracy, and for a typical calculation having $n = 80$ and $m = 8$ they are accurate to at least 10 decimal places.

Hansen & Kelmanson [26] proved that, in the absence of surface tension, any steady, smoothly varying, two-dimensional solution is necessarily symmetric about the horizontal diameter $\theta = 0,\ \pi$. Having verified this property with our preliminary numerical calculations we subsequently solved the problem only on $0 \leq \theta \leq \pi$. As we have already seen, such a symmetric solution is possible only if the weight of fluid does not exceed a critical value, which we denote by W_c. We can determine W_c from the present numerical calculation by exploiting the fact that for $W \leq W_c$ the Newton iteration converges, but for $W > W_c$ it does not. A robust way of calculating W_c is to use a bisection method, in which the interval $(W_{\rm conv}, W_{\rm div})$, where $W_{\rm conv}$ and $W_{\rm div}$ are the current values of the largest converged and smallest diverged values of W, is continually halved. Rigorous numerical testing showed that the resulting values of W_c are accurate to at least 10 decimal places.

3.3 Numerical results

Figure 2(a) shows numerically calculated solutions for h for both coating and rimming flow in the case $\delta = 0.1$ plotted as functions of θ/π for a range of values of W up to and including the respective critical values. For comparison figure 2(a) also shows Moffatt's leading-order critical solution in the limit $\delta \to 0$. Figure 2(b) shows the detail near $\theta = 0$ of numerically calculated critical solutions for h for both coating and rimming flow plotted as functions of θ for a range of values of δ and clearly illustrates the appearance of a region near $\theta = 0$ in which h'' becomes large in the limit $\delta \to 0$. Careful measurements of the curves in Figure 2(b) suggested that this region is of width $O(\delta^{2/3})$ and that within it $h = 1 + O(\delta^{2/3})$. This was confirmed both by plotting $(h-1)\delta^{-2/3}$ as

a function of $\theta\delta^{-2/3}$ near $\theta = 0$ for a range of (small) values of δ and verifying that the curves were essentially independent of δ, and by the asymptotic analysis described in §4. In particular, this means that $h = O(1)$, $h' = O(1)$ and $h'' = O(\delta^{-2/3})$ near $\theta = 0$. Note, however, this does *not* mean that the curvature of the free surface κ becomes large in the limit $\delta \to 0$. On the contrary, in general $\kappa \sim 1-\delta(h+h'')$ and so near $\theta = 0$ the curvature of the free surface is given by $\kappa = 1 + O(\delta^{1/3})$ and hence takes the finite value of unity (equal to the curvature of the cylinder) at leading order in δ. Thus (in agreement with Hansen & Kelmanson's [26] numerical results) *even in the absence of surface-tension effects*, the corner predicted by Moffatt's leading-order solution *never actually occurs.* These statements are confirmed by Figure 3(a) which shows the numerically calculated shape of the critical free surface in coating flow for a range of values of δ, and by figures 3(b) and 3(c) which show the region near $\theta = 0$ magnified 5 and 25 times respectively.

4 Asymptotic solution in the limit $\delta \to 0$

In this section we obtain higher-order corrections to Moffatt's [1] leading-order critical solution, and in particular to his value for the critical weight, in the thin-film limit $\delta \to 0$. For brevity, we give the details of this calculation only for coating flow and then indicate how the corresponding results for rimming flow can be deduced. As we have already seen, $\delta^{1/3}$ rather than simply δ is the appropriate expansion parameter in this limit, and so we write $\epsilon = \delta^{1/3}$ and pose the asymptotic expansions

$$\left.\begin{aligned} h(\theta) = \sum_{i=0}^{\infty} \epsilon^i H_i(\theta), \quad u(y,\theta) = \sum_{i=0}^{\infty} \epsilon^i U_i(y,\theta), \\ v(y,\theta) = \sum_{i=0}^{\infty} \epsilon^i V_i(y,\theta), \quad p(y,\theta) = \sum_{i=0}^{\infty} \epsilon^i P_i(y,\theta) \end{aligned}\right\} \tag{23}$$

as $\epsilon \to 0$; correspondingly we find that

$$Q = \sum_{i=0}^{\infty} \epsilon^i Q_i. \tag{24}$$

Our prime aim is to determine the critical weight W_c over all allowed values of the flux Q; we shall do this to order ϵ^4 and so, for the sake of brevity, in what follows we shall

retain only those terms needed to calculate W_c to this order.

Substituting (23) and (24) into (3)–(10) we find at leading order that

$$U_{0\theta} + V_{0y} = 0, \quad P_{0y} = -\sin\theta, \quad U_{0yy} = \cos\theta, \tag{25}$$

$$U_0 = 1, \quad V_0 = 0 \quad \text{on} \quad y = 0, \tag{26}$$

$$P_0 = 0, \quad U_{0y} = 0 \quad \text{on} \quad y = H_0(\theta). \tag{27}$$

Thus we recover Moffatt's family of solutions

$$\left.\begin{aligned} U_0 &= 1 + \left(\tfrac{1}{2}y^2 - yH_0\right)\cos\theta, \quad Q_0 = H_0 - \tfrac{1}{3}H_0^3\cos\theta, \\ V_0 &= \left(\tfrac{1}{6}y^3 - \tfrac{1}{2}H_0y^2\right)\sin\theta + \tfrac{1}{2}H_0'y^2\cos\theta, \quad P_0 = (H_0 - y)\sin\theta, \end{aligned}\right\} \tag{28}$$

parameterized by Q_0, where a prime again denotes $\mathrm{d}/\mathrm{d}\theta$. As Moffatt showed, this solution gives a continuous film encircling the cylinder only if $0 < Q_0 \leq \frac{2}{3}$; the appropriate branch of the solution H_0 in (28) may be written in the explicit form

$$H_0(\theta) = \begin{cases} \dfrac{2}{\sqrt{\cos\theta}}\cos\left(\dfrac{2\pi}{3} - \dfrac{1}{3}\cos^{-1}K(\theta)\right) & \text{if } \cos\theta > 0, \\ Q_0 & \text{if } \cos\theta = 0, \\ \dfrac{2}{\sqrt{|\cos\theta|}}\sinh\left(\dfrac{1}{3}\sinh^{-1}K(\theta)\right) & \text{if } \cos\theta < 0, \end{cases} \tag{29}$$

where

$$K(\theta) = -\tfrac{3}{2}\operatorname{sgn}(\cos\theta)\,Q_0\sqrt{|\cos\theta|} \tag{30}$$

(O'Brien & Gath [21], Duffy & Wilson [15]). The leading-order film thickness H_0 has top-to-bottom symmetry, is thickest at $\theta = 0$, thinnest at $\theta = \pi$, and takes the value Q_0 at $\theta = \pm\frac{1}{2}\pi$. The weight of fluid on the cylinder is given by $W = W_0 + O(\epsilon)$, where

$$W_0 = \int_0^{2\pi} H_0 \,\mathrm{d}\theta. \tag{31}$$

Numerical evaluation of (31) reveals that W_0 increases monotonically (indeed almost linearly) with Q_0, so that the value of Q_0 that corresponds to the critical value of W_0 is $Q_0 = Q_{0c} = \frac{2}{3}$, and with this value the critical weight of fluid is found to be $W_c = W_{0c} + O(\epsilon)$, where

$$W_{0c} \approx 4.44272. \tag{32}$$

When $W < W_c$ (and hence $Q < Q_c$) higher-order corrections to Moffatt's leading-order solution can be calculated straightforwardly as a uniformly valid regular perturbation expansion in powers of δ as described by, for example, Johnson [20] and Hosoi & Mahadevan [24]. However, as Moffatt described, when $Q_0 = Q_{0c} = \frac{2}{3}$ (but not otherwise) the film thickness (29) has a discontinuity in slope (that is, a corner) at $\theta = 0$, specifically

$$H_0 = 1 - \frac{|\theta|}{\sqrt{6}} + O(\theta^2) \quad \text{as} \quad |\theta| \to 0. \tag{33}$$

This behaviour of the leading-order solution suggests that in the critical case (but not otherwise) there is an "inner" region near $\theta = 0$ in which a more careful analysis is required. As we have already seen our numerical calculations strongly suggest (and the present asymptotic analysis will confirm) that such a region is indeed present and has width of $O(\epsilon^2)$. We therefore regard (23) as outer expansions (valid away from $\theta = 0$) and pose the inner expansions

$$\left.\begin{aligned} h(\theta) = \sum_{i=0}^{\infty} \epsilon^i h_i(\phi), \quad u(y,\theta) = \sum_{i=0}^{\infty} \epsilon^i u_i(y,\phi), \\ v(y,\theta) = \sum_{i=0}^{\infty} \epsilon^i v_i(y,\phi), \quad p(y,\theta) = \sum_{i=0}^{\infty} \epsilon^i p_i(y,\phi) \end{aligned}\right\} \tag{34}$$

near $\theta = 0$, in terms of the suitably scaled inner variable $\phi = \theta/\epsilon^2$. Note that since Q is independent of θ, equation (24) still holds in the inner region.

When $Q_0 = Q_{0c} = \frac{2}{3}$ the leading-order inner problem is

$$u_{0\phi} = 0, \quad p_{0y} = 0, \quad u_{0yy} = 1, \tag{35}$$

$$u_0 = 1 \quad \text{on} \quad y = 0, \tag{36}$$

$$p_0 = 0, \; u_{0y} = 0 \quad \text{on} \quad y = h_0(\phi), \tag{37}$$

yielding the leading-order inner solution

$$h_0 = 1, \quad u_0 = 1 - y + \tfrac{1}{2}y^2, \quad p_0 = 0. \tag{38}$$

With (38) used to simplify expressions the order-ϵ inner problem is

$$u_{1\phi} = 0, \quad p_{1y} = 0, \quad u_{1yy} = 0, \tag{39}$$

$$u_1 = 0 \quad \text{on} \quad y = 0, \tag{40}$$

$$p_1 = 0, \; u_{1y} = -h_1 \quad \text{on} \quad y = 1, \tag{41}$$

leading to

$$h_1 = \text{constant}, \quad u_1 = -h_1 y, \quad p_1 = 0, \quad Q_1 = 0. \tag{42}$$

Since $Q_1 = 0$ the order-ϵ outer problem is found to have the trivial solution

$$H_1 = 0, \quad U_1 = 0, \quad P_1 = 0, \tag{43}$$

and so (42) collapses to

$$h_1 = 0, \quad u_1 = 0, \quad p_1 = 0, \quad Q_1 = 0. \tag{44}$$

Note that the inner solutions (38) and (44) are simply the appropriate outer solutions (28) and (43) evaluated at $\theta = 0$.

The order-ϵ^2 inner problem is

$$v_{0y} + u_{2\phi} = 0, \quad p_{2y} = -\phi, \quad u_{2yy} = 0, \tag{45}$$

$$v_0 = 0, \; u_2 = 0 \quad \text{on} \quad y = 0, \tag{46}$$

$$p_2 = 0, \; u_{2y} = -h_2 \quad \text{on} \quad y = 1, \tag{47}$$

leading to

$$v_0 = \tfrac{1}{2} h_{2\phi} y^2, \quad u_2 = -h_2 y, \quad p_2 = (1 - y)\phi, \quad Q_2 = 0. \tag{48}$$

Since $Q_2 = 0$ the order-ϵ^2 outer problem is found to have the trivial solution

$$H_2 = 0, \quad P_2 = 0, \quad U_2 = 0. \tag{49}$$

The order-ϵ^3 inner problem gives

$$p_{3y} = h_{2\phi}, \quad u_{3yy} = 2(1 - y), \tag{50}$$

$$u_3 = 0 \quad \text{on} \quad y = 0, \tag{51}$$

$$p_3 = 2h_{2\phi}, \; u_{3y} = \tfrac{1}{2} - h_3 \quad \text{on} \quad y = 1, \tag{52}$$

leading to

$$u_3 = -(\tfrac{1}{2} + h_3)y + y^2 - \tfrac{1}{3}y^3, \quad p_3 = (y+1)h_{2\phi}, \quad Q_3 = 0. \tag{53}$$

The order-ϵ^3 outer problem is

$$P_{3y} = H_0' \cos\theta - (H_0 - y)\sin\theta, \quad U_{3yy} = 2(H_0 - y)\cos\theta + H_0' \sin\theta, \tag{54}$$

$$U_3 = 0 \quad \text{on} \quad y = 0, \tag{55}$$

$$\left.\begin{aligned} P_3 &= (H_3 - H_0^2)\sin\theta + 2H_0 H_0' \cos\theta, \\ U_{3y} &= 1 - \tfrac{1}{2}(H_0^2 + 2H_3)\cos\theta, \end{aligned}\right\} \quad \text{on} \quad y = H_0, \tag{56}$$

leading to

$$\left.\begin{aligned} U_3 &= y - H_0'(H_0 y - \tfrac{1}{2}y^2)\sin\theta - \left[(H_0^2 - H_0'^2)\, y - H_0 y^2 + \tfrac{1}{3}y^3\right]\cos\theta, \\ P_3 &= -\left(H_0^2 + H_0'^2 + H_0 y - \tfrac{1}{2}y^2\right)\sin\theta + (H_0 + y)H_0' \cos\theta, \\ H_3 &= -\tfrac{1}{2}H_0^2 - H_0'^2, \end{aligned}\right\} \tag{57}$$

use having been made of the fact that $Q_3 = 0$.

The order-ϵ^4 inner problem gives

$$u_{4yy} = -\tfrac{1}{2}\phi^2 + (1 + 2y)h_{2\phi\phi}, \tag{58}$$

$$u_4 = 0 \quad \text{on} \quad y = 0, \tag{59}$$

$$u_{4y} = -h_4 - \tfrac{1}{2}h_{2\phi\phi} \quad \text{on} \quad y = 1, \tag{60}$$

so that

$$u_4 = \tfrac{1}{4}\phi^2(2y - y^2) + h_{2\phi\phi}(\tfrac{1}{3}y^3 + \tfrac{1}{2}y^2 - \tfrac{5}{2}y) - h_4 y \tag{61}$$

and

$$Q_4 = -h_{2\phi\phi} - h_2^2 + \tfrac{1}{6}\phi^2. \tag{62}$$

The order-ϵ^4 outer problem gives

$$U_{4yy} = 0, \tag{63}$$

$$U_4 = 0 \quad \text{on} \quad y = 0, \tag{64}$$

$$U_{4y} = -H_4 \cos\theta \quad \text{on} \quad y = H_0, \tag{65}$$

leading to

$$U_4 = -H_4 y \cos\theta, \quad H_4 = \frac{Q_4}{1 - H_0^2 \cos\theta}. \tag{66}$$

Summarizing thus far, we have derived the expansion

$$Q = \tfrac{2}{3} + \epsilon^4 Q_4 + O(\epsilon^5) \tag{67}$$

for Q (with Q_4 unknown as yet), the outer expansion

$$h = H_0(\theta) + \epsilon^3 H_3(\theta) + \epsilon^4 H_4(\theta) + O(\epsilon^5) \tag{68}$$

for h (where H_0, H_3 and H_4 are given by (29), (57) and (66) respectively), and the inner expansion

$$h = 1 + \epsilon^2 h_2(\phi) + O(\epsilon^3), \tag{69}$$

for h, where $\phi = \theta/\epsilon^2$ and h_2 is a solution of the second-order ordinary differential equation

$$h_{2\phi\phi} + h_2^2 - \tfrac{1}{6}\phi^2 + Q_4 = 0, \tag{70}$$

subject to the matching conditions

$$h_2 \sim -\frac{|\phi|}{\sqrt{6}} \quad \text{as} \quad |\phi| \to \infty. \tag{71}$$

As we shall see shortly, higher-order terms in (69) are not needed for determining the order-ϵ^4-accurate approximation to W_c. Note that, whereas Q_1, Q_2 and Q_3 are determined by solving the inner problems at the respective orders, Q_4 is not so simply determined, but rather plays a role like Q_0 in the leading-order problem (28) in that there are different film thicknesses h_2 and H_4 (with different weights) for different values of Q_4, and the critical value of Q_4, denoted by Q_{4c}, is determined by maximising the coefficient of ϵ^4 in the asymptotic expansion of W over all allowed values of Q_4.

The system (70) and (71) for h_2 must be solved numerically for a given Q_4. Differential equations of the type (70) with similar or identical boundary conditions have been studied in other physical contexts, namely combustion theory and resonant oscillations

of water waves; see, for example, the work of Holmes [30], Ockendon, Ockendon & Johnson [31], Byatt-Smith [32, 33], Amick & Toland [34] and the summary by Sachdev ([35], §2.4). In particular, Holmes [30] proved rigorously that in the special case $Q_4 = 0$ the system (70) and (71) has two solutions; subsequent numerical calculations by Ockendon *et al.* [31] for the general case $Q_4 \neq 0$ (confirmed by our own numerical studies) indicate that there is a maximum value $Q_4 = Q_4^* \approx 0.44410$ such that the system (70) and (71) has two solutions when $Q < Q_4^*$, one solution when $Q = Q_4^*$, and no solution when $Q > Q_4^*$.

In order to calculate and then maximise the weight it is first necessary to construct an appropriate uniformly valid composite expansion for h. Since H_0, H_3 and H_4 have the asymptotic forms

$$\left.\begin{aligned} H_0 &= 1 - \frac{|\theta|}{\sqrt{6}} + \frac{2\theta^2}{9} + O(\theta^3), \\ H_3 &= -\frac{2}{3} + O(\theta), \\ H_4 &= \frac{\sqrt{6}Q_4}{2|\theta|} + \frac{Q_4}{6} + O(\theta), \end{aligned}\right\} \quad \text{as} \quad |\theta| \to 0, \tag{72}$$

a uniformly valid composite expansion for h is

$$\begin{aligned} h_{\text{comp}} = H_0(\theta) &+ \left[\hat{h}_2(\phi) + \hat{h}_2(\tilde{\phi})\right]\epsilon^2 + \left[H_3(\theta) + \hat{h}_3(\phi) + \hat{h}_3(\tilde{\phi})\right]\epsilon^3 \\ &+ \left[\hat{H}_4(\theta) + \hat{h}_4(\phi) + \hat{h}_4(\tilde{\phi})\right]\epsilon^4 + O(\epsilon^5), \end{aligned} \tag{73}$$

where we have defined $\phi = \theta/\epsilon^2$ and $\tilde{\phi} = (2\pi - \theta)/\epsilon^2$ together with

$$\hat{h}_2(\phi) = h_2(\phi) + \frac{\phi}{\sqrt{6}}, \tag{74}$$

$$\hat{h}_3(\phi) = h_3(\phi) + \frac{2}{3}, \tag{75}$$

$$\hat{h}_4(\phi) = h_4(\phi) - \frac{2\phi^2}{9} - \frac{Q_4}{6} \tag{76}$$

(which are finite for all ϕ) and

$$\hat{H}_4(\theta) = H_4(\theta) - \frac{\sqrt{6}Q_4}{2}\left(\frac{1}{\theta} + \frac{1}{2\pi - \theta}\right) \tag{77}$$

(which is finite for $0 \leq \theta < 2\pi$). From (14) the corresponding weight of fluid W is then found to be

$$W = W_{0c} + \epsilon^3 W_{3c} + \epsilon^4 W_4(\epsilon, Q_4) + O(\epsilon^5), \tag{78}$$

where W_{0c} (which depends only on the leading-order outer solution) is given by (32), W_{3c} (which depends only on the outer solution) is given by

$$W_{3c} = \int_0^{2\pi} H_3 + \tfrac{1}{2} H_0^2 \, \mathrm{d}\theta = -\int_0^{2\pi} H_0'^2 \, \mathrm{d}\theta \approx -0.17322, \tag{79}$$

and

$$W_4 = Q_4 W_{4o} + W_{4i}, \tag{80}$$

where

$$W_{4o} = \int_0^{2\pi} \frac{\hat{H}_4}{Q_4} \, \mathrm{d}\theta \approx -0.24000 \tag{81}$$

(which depends only on the order-ϵ^4 outer solution) and

$$W_{4i} = 2 \int_0^{2\pi/\epsilon^2} \hat{h}_2 \, \mathrm{d}\phi \tag{82}$$

(which depends only on the order-ϵ^2 inner solution).

Equation (70) was solved numerically for h_2 by using a standard second-order central-finite-difference method in which the ensuing algebraic equations were solved using Newton's method. Since we are specifically interested in the behaviour of W_4 in the limit $\epsilon \to 0$ in which the upper limit in (82) becomes large, the variable of integration in (82) was first transformed from ϕ to Φ by writing $\phi = \sinh(\Phi)$ and then the integration range was discretised uniformly in Φ. The corresponding value of W_4 was calculated by evaluating (82) numerically using the trapezoidal rule. By choosing a sufficiently fine grid we ensured that the results obtained are accurate to at least 6 decimal places.

Figure 4 shows numerically calculated solutions for $\hat{h}_2$ plotted as functions of ϕ for a range of values of $Q_4 \leq Q_4^*$ in the case $\epsilon = 10^{-2}$. For this particular value of ϵ the value of Q_4 that maximises W_4 is found to be $Q_4 = Q_{4c} \approx 0.43733$; figure 4 also includes the corresponding solution for $\hat{h}_2$ in this case and the single solution for $\hat{h}_2$ in the case $Q_4 = Q_4^* \approx 0.44410$.

Figure 5 shows the corresponding numerically calculated values of W_4 plotted as functions of Q_4 for a range of values of ϵ. In each case the location of the critical value of $W_4 = W_{4c}(\epsilon)$ at $Q_4 = Q_{4c}(\epsilon)$ is marked with a filled circle. In particular, figure 5 shows that $W_4 \approx 4.38788$ at $Q_4 = 0$ on the upper branch and $W_4 \approx -0.88910$ at $Q_4 = 0$ on the lower branch for these values of ϵ, and that $W_{4c} = O(\log \epsilon)$ and $Q_{4c} \to Q_4^{*-}$ in the limit $\epsilon \to 0$.

Our numerical solutions of (70) and (71) for h_2 indicate that as $Q_4 \to Q_4^{*-}$ on the upper branch

$$h_2 = h_{2,0}(\phi) + (Q_4^* - Q_4)^{\frac{1}{2}} h_{2,1}(\phi) + (Q_4^* - Q_4) h_{2,2}(\phi) + o(Q_4^* - Q_4), \tag{83}$$

where $h_{2,0}$ is the (unique) solution for h_2 when $Q_4 = Q_4^*$. Substituting (83) into (70) and the far-field condition

$$h_2 = -\frac{\phi}{\sqrt{6}} + \frac{3Q_4}{\sqrt{6}\phi} + \frac{9Q_4^2}{2\sqrt{6}\phi^3} + \frac{3Q_4}{\phi^4} + O\left(\frac{1}{\phi^5}\right) \quad \text{as} \quad \phi \to \infty, \tag{84}$$

we find that $h_{2,1}$ satisfies

$$h_{2,1\phi\phi} + 2h_{2,0}h_{2,1} = 0 \tag{85}$$

subject to

$$h_{2,1} = O\left(\phi^{-\frac{1}{4}} \exp\left[-\left(\frac{2}{3}\right)^{\frac{5}{4}} \phi^{\frac{3}{2}}\right]\right) \quad \text{as} \quad \phi \to \infty, \tag{86}$$

and that $h_{2,2}$ satisfies

$$h_{2,2\phi\phi} + 2h_{2,0}h_{2,2} = 1 - h_{2,1}^2 \tag{87}$$

subject to

$$h_{2,2} = -\frac{\sqrt{6}}{2\phi} - \frac{9Q_4^*}{\sqrt{6}\phi^3} - \frac{3}{\phi^4} + O\left(\frac{1}{\phi^5}\right) \quad \text{as} \quad \phi \to \infty. \tag{88}$$

Substituting (83) into (80) yields

$$W_4 = Q_4^* W_{4o} + I_0 + I_1 (Q_4^* - Q_4)^{\frac{1}{2}} + (I_2 - W_{4o})(Q_4^* - Q_4) + o(Q_4^* - Q_4), \tag{89}$$

where

$$I_0 = 2\int_0^{2\pi/\epsilon^2} h_{2,0} + \frac{\phi}{\sqrt{6}}\, \mathrm{d}\phi, \tag{90}$$

$$I_1 = 2\int_0^{2\pi/\epsilon^2} h_{2,1}\,\mathrm{d}\phi, \tag{91}$$

$$I_2 = 2\int_0^{2\pi/\epsilon^2} h_{2,2}\,\mathrm{d}\phi. \tag{92}$$

From (84), (86) and (88) we can deduce that

$$I_0 = -2\sqrt{6}Q_4^*\log\epsilon + A_0 + O(\epsilon^4), \tag{93}$$

$$I_1 = A_1 + o(1), \tag{94}$$

$$I_2 = 2\sqrt{6}\log\epsilon + A_2 + O(\epsilon^4) \tag{95}$$

as $\epsilon \to 0$, where A_0, A_1 and A_2 are constants. Determining Q_{4c} by solving $\mathrm{d}W_4/\mathrm{d}Q_4 = 0$ in (89) for Q_4 yields

$$Q_{4c} = Q_4^* - \left(\frac{\frac{1}{2}A_1}{2\sqrt{6}\log\epsilon + A_2 - W_{4o}}\right)^2 + o(\log\epsilon)^{-3} \tag{96}$$

and

$$W_{4c} = -2\sqrt{6}Q_4^*\log\epsilon + Q_4^*W_{4o} + A_0 - \frac{\left(\frac{1}{2}A_1\right)^2}{2\sqrt{6}\log\epsilon + A_2 - W_{4o}} + o(\log\epsilon)^{-2} \tag{97}$$

as $\epsilon \to 0$. Our numerical solutions for h_2 yield $Q_4^*W_{4o} + A_0 \approx 3.17807$, $\left(\frac{1}{2}A_1\right)^2 \approx 4.56356$ and $A_2 - W_{4o} \approx -3.55719$. Hence the main theoretical results of the present work, namely the asymptotic solutions for Q_c and W_c in the limit $\epsilon \to 0$, are given by

$$Q_c = Q_{0c} + \epsilon^4 Q_{4c} + o(\epsilon^4(\log\epsilon)^{-3}), \tag{98}$$

where $Q_{0c} = \frac{2}{3}$ and Q_{4c} is given by (96), and

$$W_c = W_{0c} + \epsilon^3 W_{3c} + \epsilon^4 W_{4c} + o(\epsilon^4(\log\epsilon)^{-2}), \tag{99}$$

where W_{0c}, W_{3c} and W_{4c} are given by (32), (79) and (97), respectively.

Note that while W_{0c} and W_{3c} can be determined without a detailed knowledge of the solution in the inner region, the higher-order terms cannot. In particular, W_{4c} can be obtained only by calculating the leading-order solution in the inner region as we have done here. As we shall see in the next section, in practice the $\epsilon^4 W_{4c}$ term dominates

the formally lower-order $\epsilon^3 W_{3c}$ term and so it must be included in order to obtain an accurate correction to W_{0c}.

The above results are for coating flow. The corresponding results for rimming flow are obtained by replacing p with $-p$ and ϵ with $-\epsilon$ (and so δ with $-\delta$) everywhere except (since W_{4i} is insensitive to replacing ϵ with $-\epsilon$) in $\log \epsilon$.

One of the features of the present analysis is that it entirely neglects the effects of both inertia and surface tension. It is therefore important to determine under what conditions these assumptions are valid. From Hosoi & Mahadevan's [24] equation (2.19) we can deduce that inertia and surface-tension effects will not appear in the $O(\epsilon^4)$ inner problem provided that

$$\frac{a^2\omega}{\nu} \ll \epsilon^{-2} = \left(\frac{\nu\omega}{ga}\right)^{-1/3}, \tag{100}$$

$$\frac{\sigma}{\rho g a^2} \ll \epsilon^5 = \left(\frac{\nu\omega}{ga}\right)^{5/6}, \tag{101}$$

respectively, where σ denotes the coefficient of surface tension. In the experiments described by Moffatt in which $\mu = 80$ g cm^{-1} s^{-1}, $a = 2.04$ cm and $\rho \simeq 1$ g cm^{-3} both (100) and (101) are well satisfied. Specifically (100) holds provided that $\omega \ll 196$ rpm compared to a largest reported value of $\omega = 77.4$ rpm, while with $\omega = 8$ rpm (the smallest reported value of ω) (101) holds provided that $\sigma \ll 241$ dyn cm^{-1}. Moffatt does not give a value for σ, but the experimental data given by Balmer & Wang [4] suggests it would almost certainly be below 100 dyn cm^{-1}. In the experiments described by Kelmanson [28] using a smaller cylinder and less viscous fluids (100) is again well satisfied, but (101) is at best only marginally satisfied, indicating that surface-tension effects may play a significant role near $\theta = 0$ in these experiments.

5 Comparison between numerical, asymptotic and experimental results

Figure 6 shows the excellent agreement between W_{4c} given by (97) and the numerically calculated values of $(W_c - W_{0c} - \epsilon^3 W_{3c})/\epsilon^4$ for both coating and rimming flow. The figure also shows $-2\sqrt{6}Q_4^* \log\epsilon + Q_4^* W_{4o} + A_0 \approx -2.17562 \log\epsilon + 3.17807$, from which the significant contribution of the final term in (97) can be ascertained.

Figure 7 shows the excellent agreement between the leading-order asymptotic and numerically calculated critical values of $h - H_0 - \epsilon^3 H_3$ when $Q = Q_c$ in the case $\epsilon = 10^{-3/2}$ for both coating and rimming flow. Away from $\theta = 0$ and $\theta = 2\pi$ the leading-order asymptotic solution for this quantity is the sum of the three $O(\epsilon^4)$ terms $\epsilon^2 \hat{h}_2(\phi)$, $\epsilon^2 \hat{h}_2(\tilde{\phi})$ and $\epsilon^4 \hat{H}_4(\theta)$, and hence in figure 7($a$) $(h - H_0 - \epsilon^3 H_3)/\epsilon^4$ is plotted as a function of $\theta/2\pi$ from 0 to 1. Figure 7(a) also shows the individual contributions of the terms $\epsilon^2 \hat{h}_2(\phi)$, $\epsilon^2 \hat{h}_2(\tilde{\phi})$ and $\epsilon^4 \hat{H}_4(\theta)$ separately. Near $\theta = 0$ the leading-order asymptotic solution is given by just the $O(\epsilon^2)$ term $\epsilon^2 \hat{h}_2(\phi)$, and hence in figure 7($b$) $(h - H_0 - \epsilon^3 H_3)/\epsilon^2$ is plotted as a function of ϕ.

Note that in figures 6 and 7 the coating and rimming results straddle the asymptotic solution, as expected.

Figures 8 and 9 show the comparison between the order-ϵ^4-accurate asymptotic solution for W_c given by (99) and the numerically calculated values of W_c for coating flow and (in figure 9) rimming flow. For consistency with earlier authors the results in figures 8 and 9 are plotted as functions of the Stokes number $\gamma = \delta^{-2} = \epsilon^{-6}$. Figure 8 also shows Hansen & Kelmanson's [26] numerical results, both the full (implicit) and the simplified (explicit) versions of Kelmanson's [28] approximate theory, and Kelmanson's [28] experimental results. The error bars on Hansen & Kelmanson's [26] numerical results are taken from figure 2 of their paper. The upper and lower ends of these error bars indicate the smallest value of W for which their numerical calculations did not converge within 200 seconds of CPU time and the largest value of W for which they

did, respectively, and the dots simply denote the mid-points between the two extreme values. Kelmanson [28] does not give any indication of the errors in his experimental results. Figure 9 shows results for both coating and rimming flow for larger values of γ (i.e. for smaller values of δ).

Figures 8 and 9 show that the asymptotic and numerically calculated solutions are in good agreement for values of γ greater than about 10, i.e. for values of δ less than about 0.3. Figure 8(a) shows that all the results are in rough agreement over the range of values of γ shown. Figure 8(b) clearly shows that while our asymptotic and numerical solutions together with Hansen & Kelmanson's [26] numerically calculated results all lie above W_{0c}, Kelmanson's [28] experimental results lie below it. Figure 8(b) also shows that while Kelmanson's [28] approximate solutions are indeed closer to Hansen & Kelmanson's [26] numerical results and Kelmanson's [28] experimental results than W_{0c}, none are in particularly good agreement with either our asymptotic or our numerically calculated solutions. In particular, in the limit $\epsilon \to 0$ both the full (implicit) and the simplified (explicit) versions of Kelmanson's [28] theory yield

$$Q_c = \frac{2}{3} + \frac{1}{2}\epsilon^3 + O(\epsilon^6), \quad W_c = \frac{4\pi}{3} + \frac{5\pi}{9}\epsilon^3 + O(\epsilon^6), \tag{102}$$

which differ from the corresponding exact asymptotic solutions given by (98) and (99) at first and leading order in ϵ^3 respectively, explaining why neither of Kelmanson's [28] approximate solutions converge to W_{0c} for larger values of γ in Fig. 8(b).

Figure 9 demonstrates that while $W_c > W_{0c}$ for all values of γ in rimming flow, in coating flow even though $W_{3c} < 0$, W_c falls below W_{0c} only when γ is larger than about 1.64×10^{11}, i.e. only when δ is smaller than about 2.47×10^{-6}. This very large value of γ (and hence very small value of δ) means that the $O(\delta^{4/3} \log \delta)$ term dominates the formally lower-order $O(\delta)$ term for all but *extremely* slow rotation rates. In particular, for the experiments described by Moffatt this will occur whenever the rotation rate is faster than approximately one rotation every 1300 years! Thus in practice the higher-order terms *must* be included in order to obtain an accurate correction to W_{0c}.

For $\gamma > 10^{12}$ the numerically calculated values of $(W_c - W_{0c})/\epsilon^3$ begin to lose significance, and so in order to demonstrate conclusively that they do indeed approach W_{3c} for coating flow and $-W_{3c}$ for rimming flow in the limit $\epsilon \to 0$, figure 9 also includes the numerically calculated values of

$$\Delta W_c = \frac{1}{2\epsilon^3}(W_c^{\text{coat}} - W_c^{\text{rim}}), \tag{103}$$

where the superscripts "coat" and "rim" denote values for coating and rimming flow respectively, confirming that $\Delta W_c \to W_{3c}$, as expected.

6 Conclusions

In the present paper we used a combination of analytical and numerical techniques to re-examine the question posed by Moffatt [1] of determining the critical weights of fluid that can be maintained per unit length in a steady, smoothly varying, two-dimensional film in either coating or rimming flow on a rotating horizontal cylinder. We used a pseudospectral method to obtain highly accurate numerical solutions for steady Stokes flow on a cylinder and hence to calculate the critical weights. In particular, these numerical calculations revealed that the behaviour of the critical solutions in the thin-film limit $\delta \to 0$ in an inner region near $\theta = 0$ (where Moffatt's leading-order outer solution has a corner) are not captured by naive outer asymptotic solutions in integer powers of δ. Motivated by these numerical results we obtained the uniformly valid critical asymptotic solutions in the thin-film limit to sufficient accuracy to enable us to calculate the critical fluxes and weights to accuracies $o(\delta^{4/3}(\log\delta)^{-3})$ and $o(\delta^{4/3}(\log\delta)^{-2})$ relative to Moffatt's leading-order values, respectively. We found that our asymptotic solutions for the critical weights are in good agreement with the numerically calculated results over a wide range of values of δ. In particular, our numerical and asymptotic calculations showed that, even in the absence of surface-tension effects, the corner predicted by Moffatt's leading-order outer solution never actually occurs. In practice the higher-order terms obtained in the present work dominate the formally lower-order term that can be

obtained straightforwardly without a detailed knowledge of the solution in the inner region, and so these higher-order terms must be included in order to obtain accurate corrections to W_{0c}. In particular, in practice the critical weights in both coating and rimming flow always exceed W_{0c}. We did not find particularly good agreement between the present asymptotic and numerically calculated solutions (which lie above Moffatt's value for the relevant values of δ) and Kelmanson's [28] experimental results (which lie below it). We should, however, bear in mind that this is not an easy experiment to perform accurately and the difference from Moffatt's value is small in absolute terms. Moreover, as we have already seen, surface-tension effects may play a significant role in these experiments. There is evidently a need for further experimental measurements of the critical weight.

Acknowledgements

The first author (SKW) gratefully acknowledges the ongoing financial support of the Leverhulme Trust via a Research Fellowship. All three authors acknowledge discussions with Dr Mark Kelmanson (University of Leeds) during the course of the present work.

References

[1] H. K. Moffatt, Behaviour of a viscous film on the outer surface of a rotating cylinder. *J. Méc.* **16** (1977) 651–673.

[2] R. T. Balmer, The hygrocyst - a stability phenomenon in continuum mechanics. *Nature* **227** (1970) 600–601.

[3] M. J. Karweit & S. Corrsin, Observations of cellular patterns in a partly filled, horizontal, rotating cylinder. *Phys. Fluids* **18** (1975) 111–112.

[4] R. T. Balmer & T. G. Wang, An experimental study of internal hygrocysts. *Trans. ASME J. Fluids Eng.* **98** (1976) 688–694.

[5] J. P. Kovac & R. T. Balmer, Experimental studies of external hygrocysts. *Trans. ASME J. Fluids Eng.* **102** (1980) 226–230.

[6] D. D. Joseph & L. Preziosi, Stability of rigid motions and coating films in bicomponent flows of immiscible liquids. *J. Fluid Mech.* **185** (1987) 323–351.

[7] L. Preziosi & D. D. Joseph, The run-off condition for coating and rimming flows. *J. Fluid Mech.* **187** (1988) 99–113.

[8] F. Melo, Localized states in a film-dragging experiment. *Phys. Rev. E* **48** (1993) 2704–2712.

[9] F. Melo & S. Douady, From solitary waves to static patterns via spatiotemporal intermittency. *Phys. Rev. Lett.* **71** (1993) 3283–3286.

[10] D. P. Vallette, W. S. Edwards & J. P. Gollub, Transition to spatiotemporal chaos via spatially subharmonic oscillations of a periodic front. *Phys. Rev. E* **49** (1994) R4783–R4786.

[11] S. T. Thoroddsen & L. Mahadevan, Shark-teeth pattern in coating flow inside a horizontally rotating cylinder. *Phys. Fluids* **8** (1996) S10.

[12] S. T. Thoroddsen & L. Mahadevan, Experimental study of coating flows in a partially-filled horizontally rotating cylinder. *Expts in Fluids* **23** (1997) 1–13.

[13] D. P. Vallette, G. Jacobs & J. P. Gollub, Oscillations and spatiotemporal chaos of one-dimensional fluid fronts. *Phys. Rev. E* **55** (1997) 4274–4287.

[14] O. A. M. Boote & P. J. Thomas, Effects of granular additives on transition boundaries between flow states of rimming flows. *Phys. Fluids* **11** (1999) 2020–2029.

[15] B. R. Duffy & S. K. Wilson, Thin-film and curtain flows on the outside of a rotating horizontal cylinder. *J. Fluid Mech.* **394** (1999) 29–49.

[16] J. J. Van Rossum, Viscous lifting and drainage of liquids. *Appl. Sci. Res. A* **7** (1958) 121–144.

[17] A. B. Ross, S. K. Wilson & B. R. Duffy, Thin-film flow of a viscoplastic material round a large horizontal stationary or rotating cylinder. *J. Fluid Mech.* **430** (2001) 309–333.

[18] W. Nusselt, Die Oberflächenkondensation des Wasserdampfes. *Z. Vereines deutscher Ingenieure* **60** (1916) 541–546 (in German).

[19] W. Nusselt, Die Oberflächenkondensation des Wasserdampfes. *Z. Vereines deutscher Ingenieure* **60** (1916) 569–575 (in German).

[20] R. E. Johnson, Steady-state coating flows inside a rotating horizontal cylinder. *J. Fluid Mech.* **190** (1988) 321–342.

[21] S. B. G. O'Brien & E. G. Gath, The location of a shock in rimming flow. *Phys. Fluids* **10** (1998) 1040–1042.

[22] M. Tirumkudulu & A. Acrivos, Coating flows within a rotating horizontal cylinder: lubrication analysis, numerical computations, and experimental measurements. *Phys. Fluids* **13** (2001) 14–19.

[23] S. D. R. Wilson & J. Williams, The flow of a liquid film on the inside of a rotating cylinder, and some related problems. *Phys. Fluids* **9** (1997) 2184–2190.

[24] A. E. Hosoi & L. Mahadevan, Axial instability of a free-surface front in a partially filled horizontal rotating cylinder. *Phys. Fluids* **11** (1999) 97–106.

[25] R. E. Johnson, Coating flow stability in rotational molding. In *Engineering Science, Fluid Dynamics: A Symposium to Honor T. Y. Wu* (ed. G. T. Yates), pp. 435–449. (World Scientific, 1990).

[26] E. B. Hansen & M. A. Kelmanson, Steady, viscous, free-surface flow on a rotating cylinder. *J. Fluid Mech.* **272** (1994) 91–107.

[27] R. C. Peterson, P. K. Jimack & M. A. Kelmanson, On the stability of viscous, free-surface flow supported by a rotating cylinder. *Proc. Roy. Soc. Lond. Ser. A* **457** (2001) 1427–1445.

[28] M. A. Kelmanson, Theoretical and experimental analyses of the maximum-supportable fluid load on a rotating cylinder. *J. Engng Maths* **29** (1995) 271–285.

[29] C. Canuto, M. Y. Hassaini, A. Quarteroni & T. A. Zang, *Spectral Methods in Fluid Dynamics*, (Springer, 1987).

[30] P. Holmes, On a second-order boundary-value problem arising in combustion theory. *Quart. Appl. Maths* **40** (1982) 53–62.

[31] H. Ockendon, J. R. Ockendon & A. D. Johnson, Resonant sloshing in shallow water. *J. Fluid Mech.* **167** (1986) 465–479.

[32] J. G. Byatt-Smith, On the solutions of a second order differential equation arising in the theory of resonant oscillations in a tank. *Studies in Appl. Maths* **79** (1988) 143–157.

[33] J. G. Byatt-Smith, The asymptotic solution of a connection problem of a second order ordinary differential equation. *Studies in Appl. Maths* **80** (1989) 109–135.

[34] C. J. Amick & J. F. Toland, A differential equation in the theory of resonant oscillations of water waves. *Proc. Roy. Soc. Edin.* **114A** (1990) 15–26.

[35] P. L. Sachdev, *A Compendium on Nonlinear Ordinary Differential Equations.* (Wiley, 1997).

Figure Captions

Figure 1 : Geometry of the coating flow problem.

Figure 2 : (a) Numerically calculated solutions for h for both coating flow (solid lines) and rimming flow (dashed lines) in the case $\delta = 0.1$ plotted as functions of θ/π for $W = 1, 2, 3, 4$ and W_c, where $W_c \approx 4.69428$ for coating flow and $W_c \approx 4.73018$ for rimming flow. The dotted curve shows Moffatt's [1] leading-order critical solution for h in the limit $\delta \to 0$ for which $W_c \approx 4.44272$. (b) Detail near $\theta = 0$ of the numerically calculated critical solutions for h for both coating flow (solid lines) and rimming flow (dashed lines) plotted as functions of θ for $\delta = 0$ and $\delta = 10^{-k/4}$ for $k = 16, 17, \ldots, 22$.

Figure 3 : Numerically calculated shape of the critical free surface in coating flow for $\delta = 10^{-k/4}$ for $k = 0, 1, 2, \ldots$. Parts (b) and (c) show the region near $\theta = 0$ magnified 5 and 25 times respectively.

Figure 4 : Numerically calculated solutions for $\hat{h}_2$ plotted as functions of ϕ for a range of values of $Q_4 \leq Q_4^*$ in the case $\epsilon = 10^{-2}$. For each value of $Q_4 < Q_4^*$ the larger solution is marked with a solid line and the smaller one with a dashed line. The figure also includes the larger solution for $\hat{h}_2$ in the case $Q_4 = Q_{4c} \approx 0.43733$ (which maximises W_4 for this particular value of ϵ) and the single solution for $\hat{h}_2$ in the case $Q_4 = Q_4^* \approx 0.44410$.

Figure 5 : Numerically calculated values of W_4 plotted as functions of Q_4 for $\epsilon = 10^{-1}$, 10^{-2} and 10^{-3}. In each case the location of the critical value of $W_4 = W_{4c}(\epsilon)$ at $Q_4 = Q_{4c}(\epsilon)$ is marked with a filled circle ($\bullet$). The vertical dashed line indicates the value $Q_4 = Q_4^* \approx 0.44410$ beyond which the system (70) and (71) has no solutions, and the sloping dashed curves (which are almost straight lines) show the centre-lines between the upper and lower branches of solutions.

Figure 6 : W_{4c} given by (97) (solid curve) and the numerically calculated values of $(W_c - W_{0c} - \epsilon^3 W_{3c})/\epsilon^4$ plotted as functions of $\delta = \epsilon^3$ for both coating flow (marked with filled circles •) and rimming flow (marked with open circles ○). The dashed curve denotes $-2.17562 \log \epsilon + 3.17807$.

Figure 7 : Leading-order asymptotic and numerically calculated critical values of (a) $(h - H_0 - \epsilon^3 H_3)/\epsilon^4$ plotted as functions of $\theta/2\pi$ and (b) $(h - H_0 - \epsilon^3 H_3)/\epsilon^2$ plotted as functions of ϕ when $Q = Q_c$ in the case $\epsilon = 10^{-3/2}$ for both coating flow (marked with filled circles •) and rimming flow (marked with open circles ○). In (a) the dashed lines denote the individual contributions of the terms $\epsilon^2 \hat{h}_2(\phi)$, $\epsilon^2 \hat{h}_2(\tilde{\phi})$ and $\epsilon^4 \hat{H}_4(\theta)$.

Figure 8 : (a) W_c and (b) $(W_c - W_{0c})/\epsilon^3$ calculated using the order-ϵ^4-accurate asymptotic solution for W_c given by (99) (dashed curve) and the numerically calculated values of W_c (solid curve) for coating flow plotted as functions of $\gamma = \delta^{-2} = \epsilon^{-6}$. The figure also shows Hansen & Kelmanson's [26] numerical results (denoted by filled circles with error bars), Kelmanson's [28] approximate theory (denoted by dash-dotted curves; the upper and lower curves denote the simplified and the full versions of the theory respectively) and Kelmanson's [28] experimental results (filled squares denote results for SAE 30 oil, open squares "Gold X" oil, and stars SAE 50 oil).

Figure 9 : $(W_c - W_{0c})/\epsilon^3$ calculated using the order-ϵ^4-accurate asymptotic solution for W_c given by (99) (dashed curve) and the numerically calculated values of W_c (solid curve) for both coating and rimming flow plotted as functions of $\gamma = \delta^{-2} = \epsilon^{-6}$. The dash-dotted line denotes the numerically calculated values of ΔW_c given by (103).

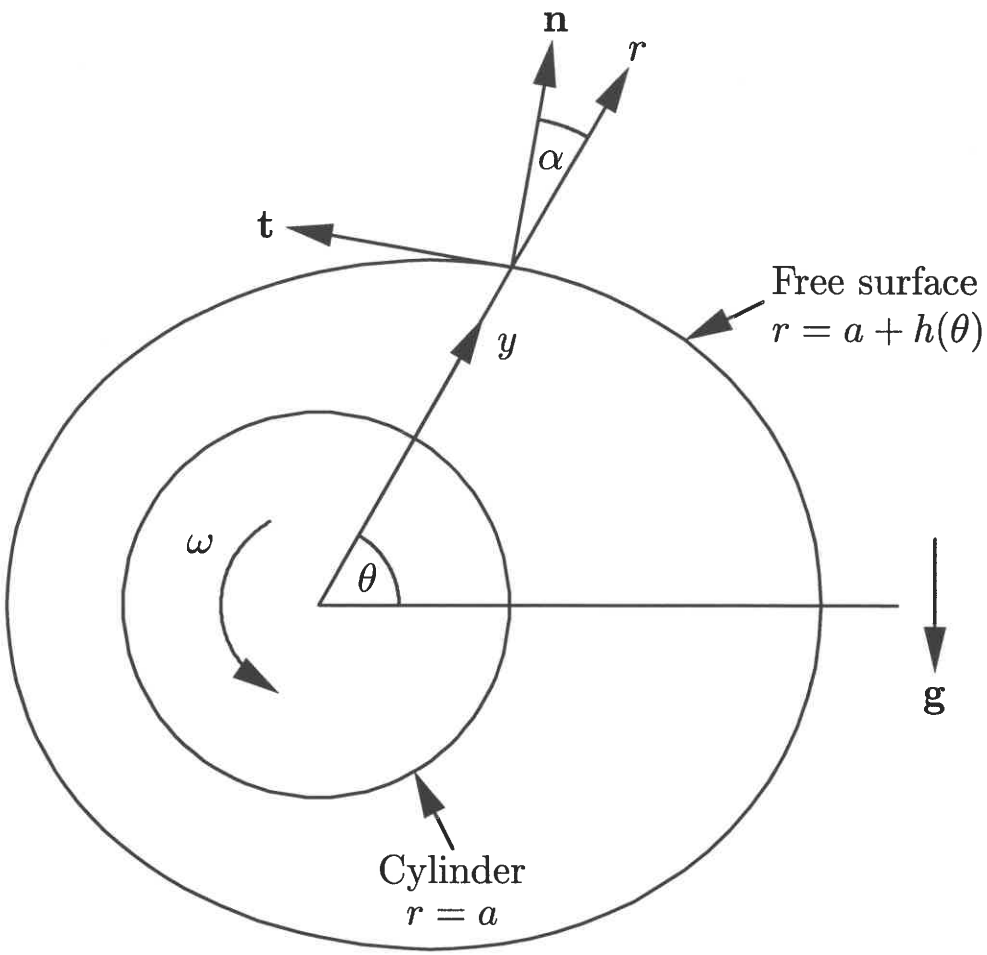

Figure 1

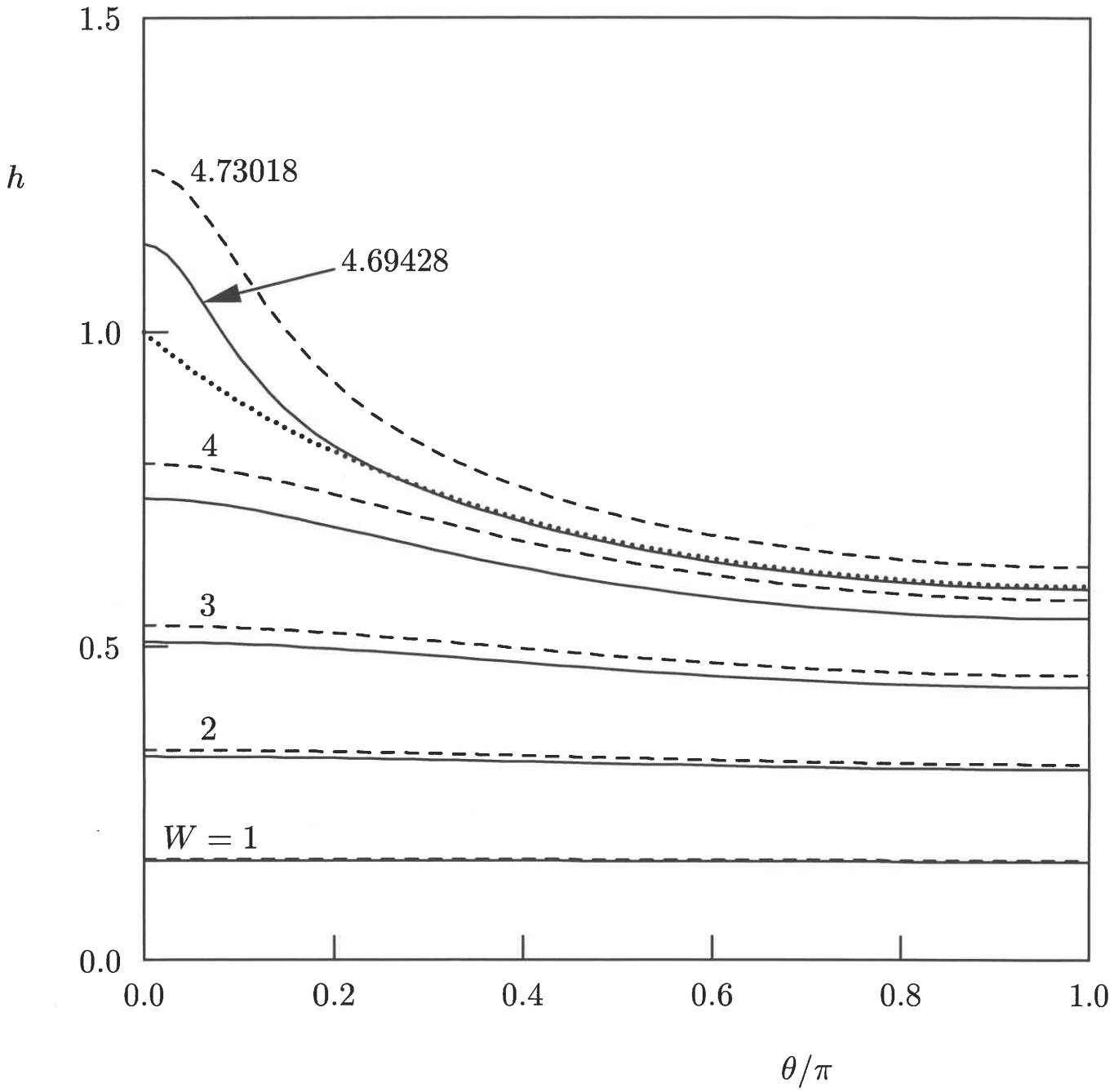

Figure 2(a)

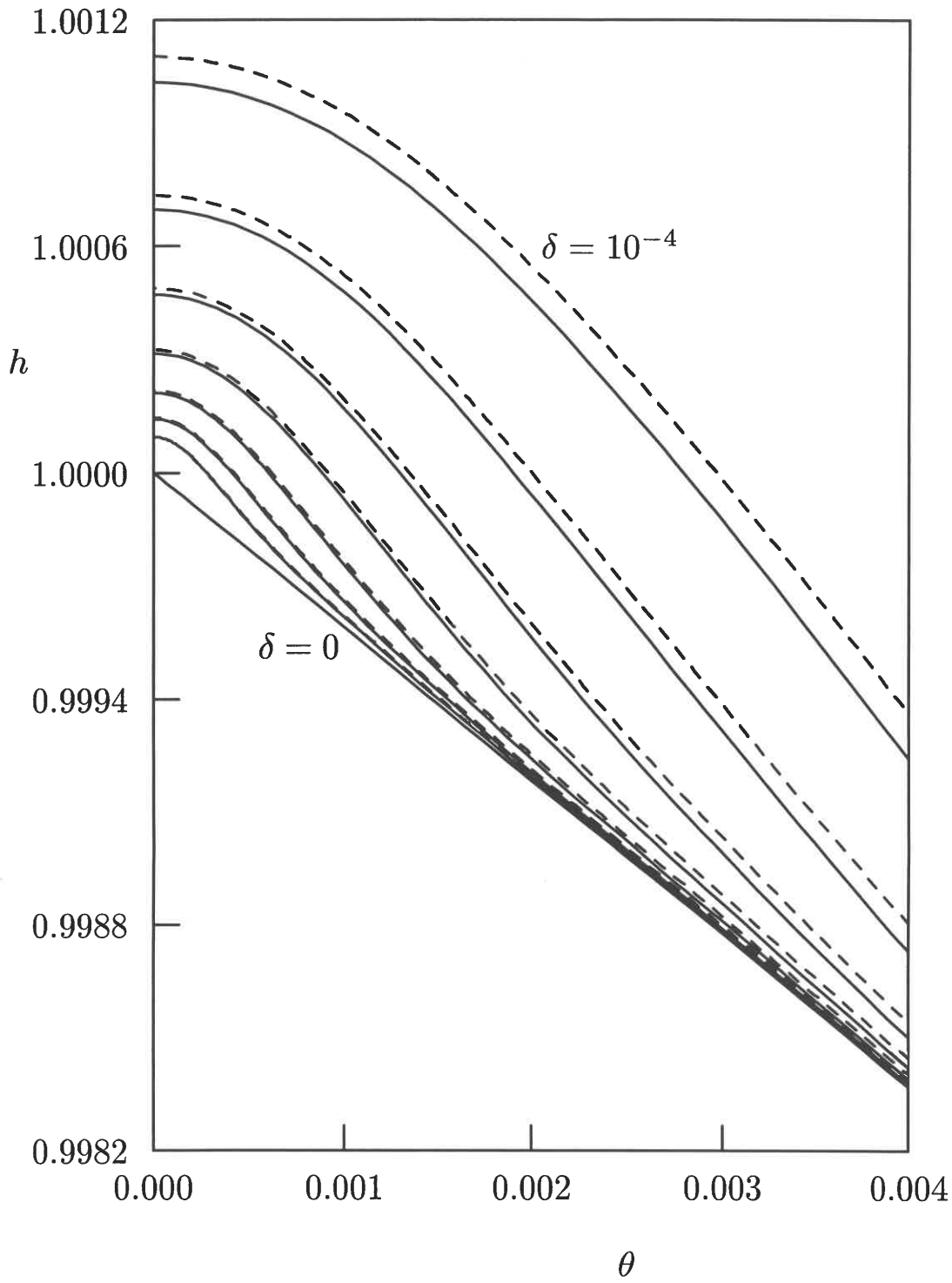
1.0012
1.0006
1.0000
0.9994
0.9988
0.9982
h
$\delta = 10^{-4}$
$\delta = 0$
0.000
0.001
0.002
0.003
0.004
θ

Figure 2(b)

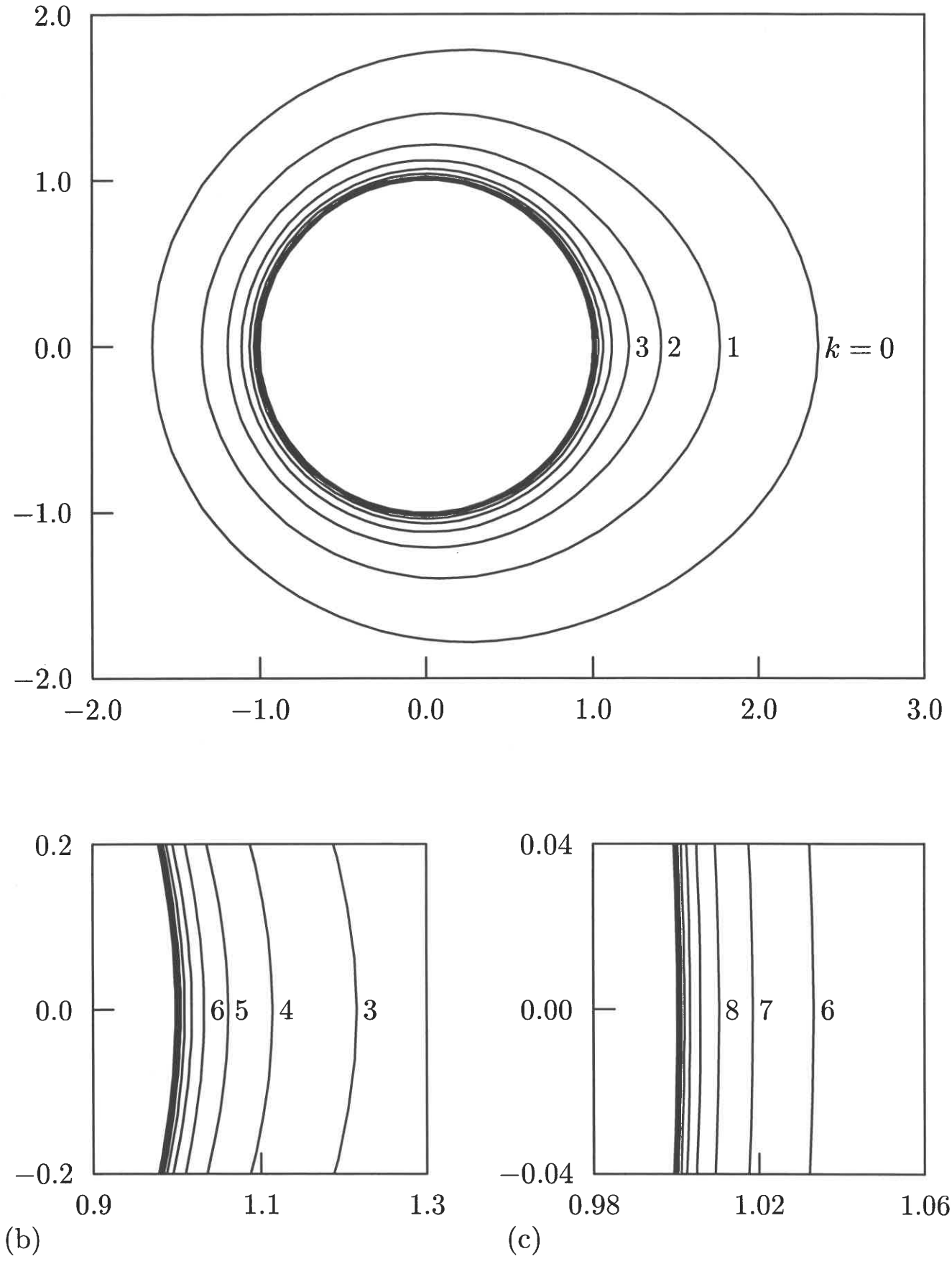
2.0
1.0
0.0
−1.0
−2.0
−2.0
−1.0
0.0
1.0
2.0
3.0
3
2
1
$k = 0$
0.2
0.0
−0.2
0.9
1.1
1.3
6
5
4
3
(b)
0.04
0.00
−0.04
0.98
1.02
1.06
8
7
6
(c)

Figure 3

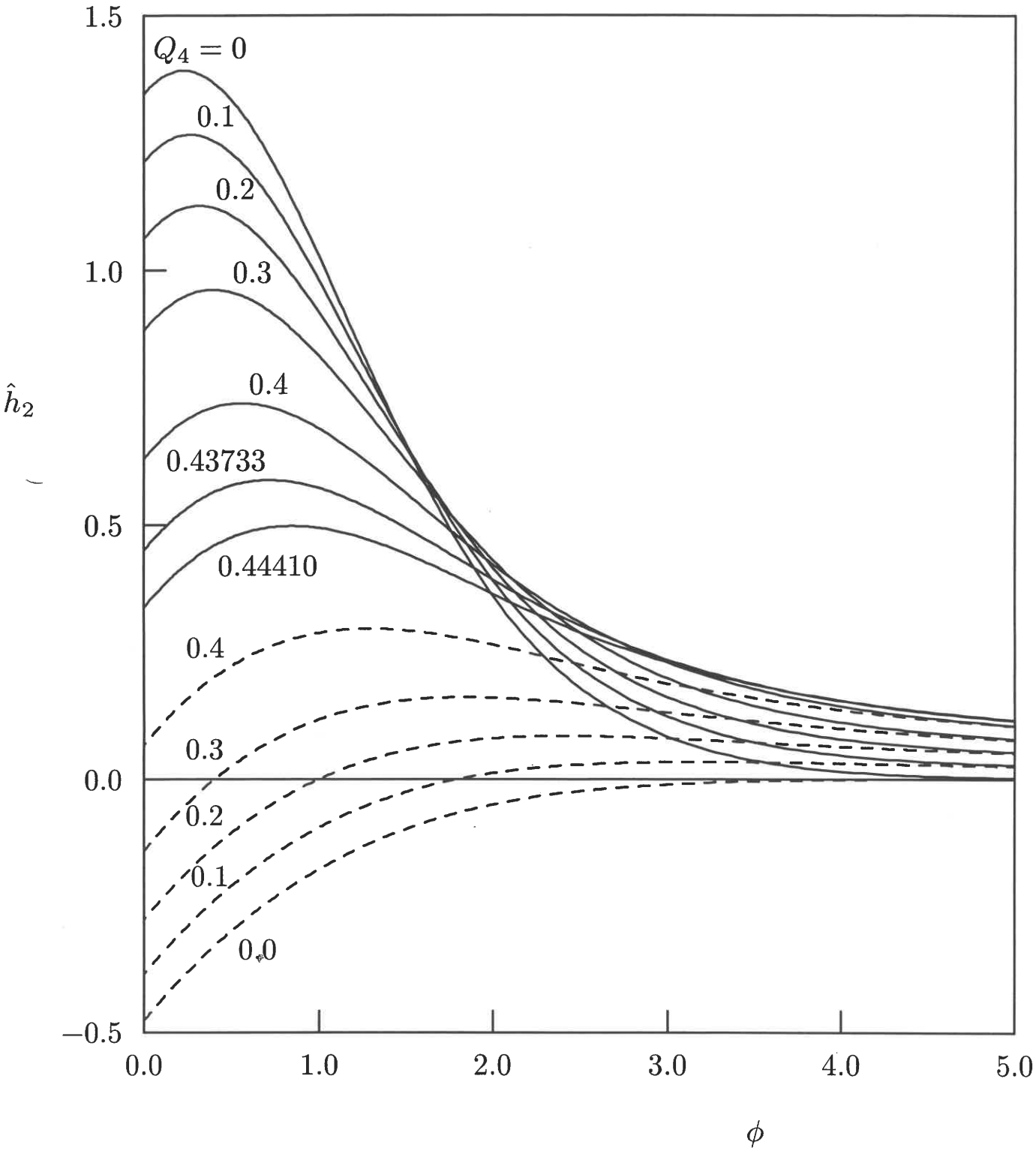
1.5
$Q_4 = 0$
0.1
0.2
1.0
0.3
0.4
$\hat{h}_2$
0.43733
0.5
0.44410
0.4
0.3
0.0
0.2
0.1
0.0
−0.5
0.0
1.0
2.0
3.0
4.0
5.0
ϕ

Figure 4

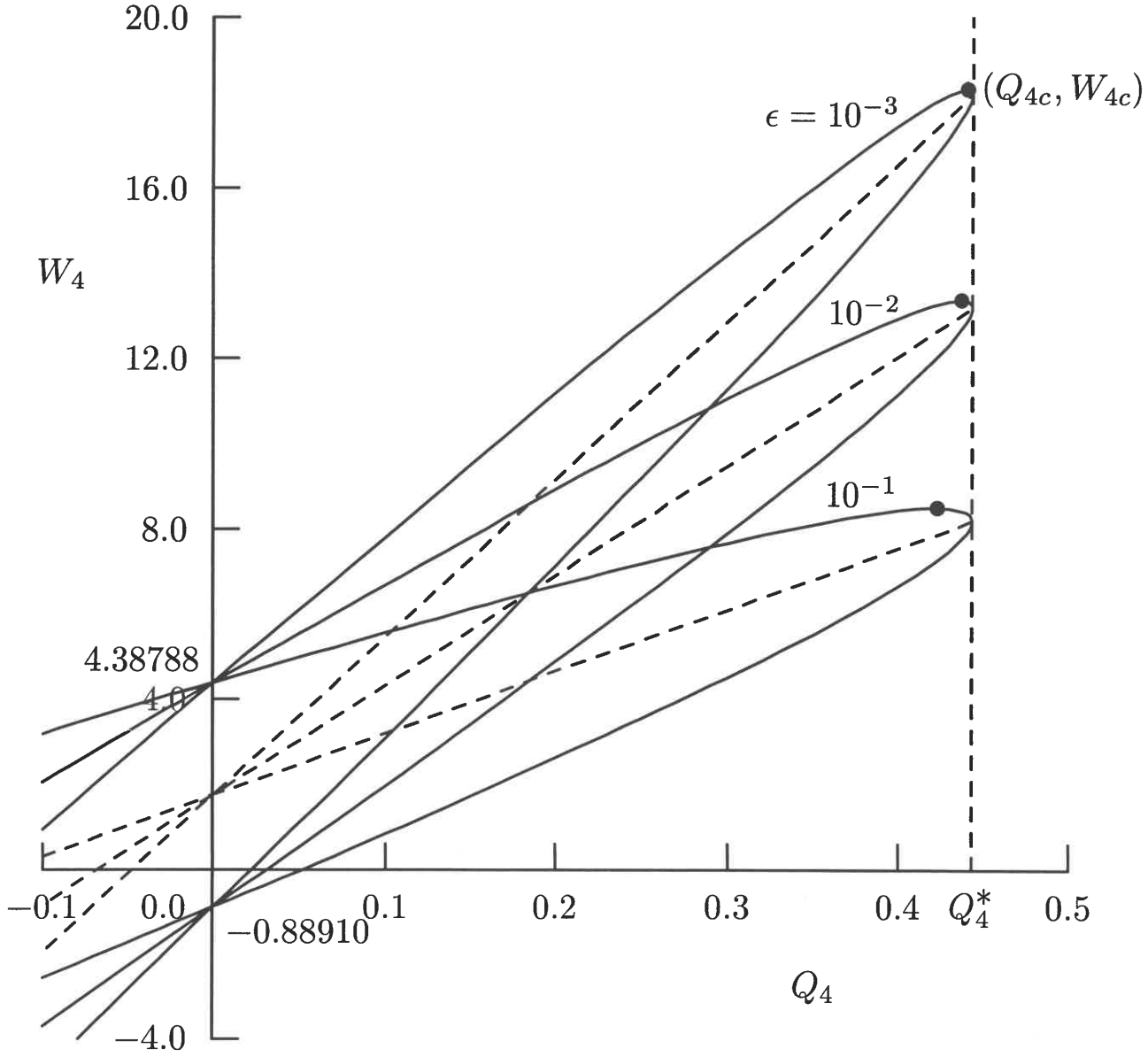
20.0
16.0
W_4
12.0
8.0
4.38788
4.0
$\epsilon = 10^{-3}$
(Q_{4c}, W_{4c})
10^{-2}
10^{-1}
−0.1
0.0
−0.88910
0.1
0.2
0.3
0.4
Q_4^*
0.5
Q_4
−4.0

Figure 5

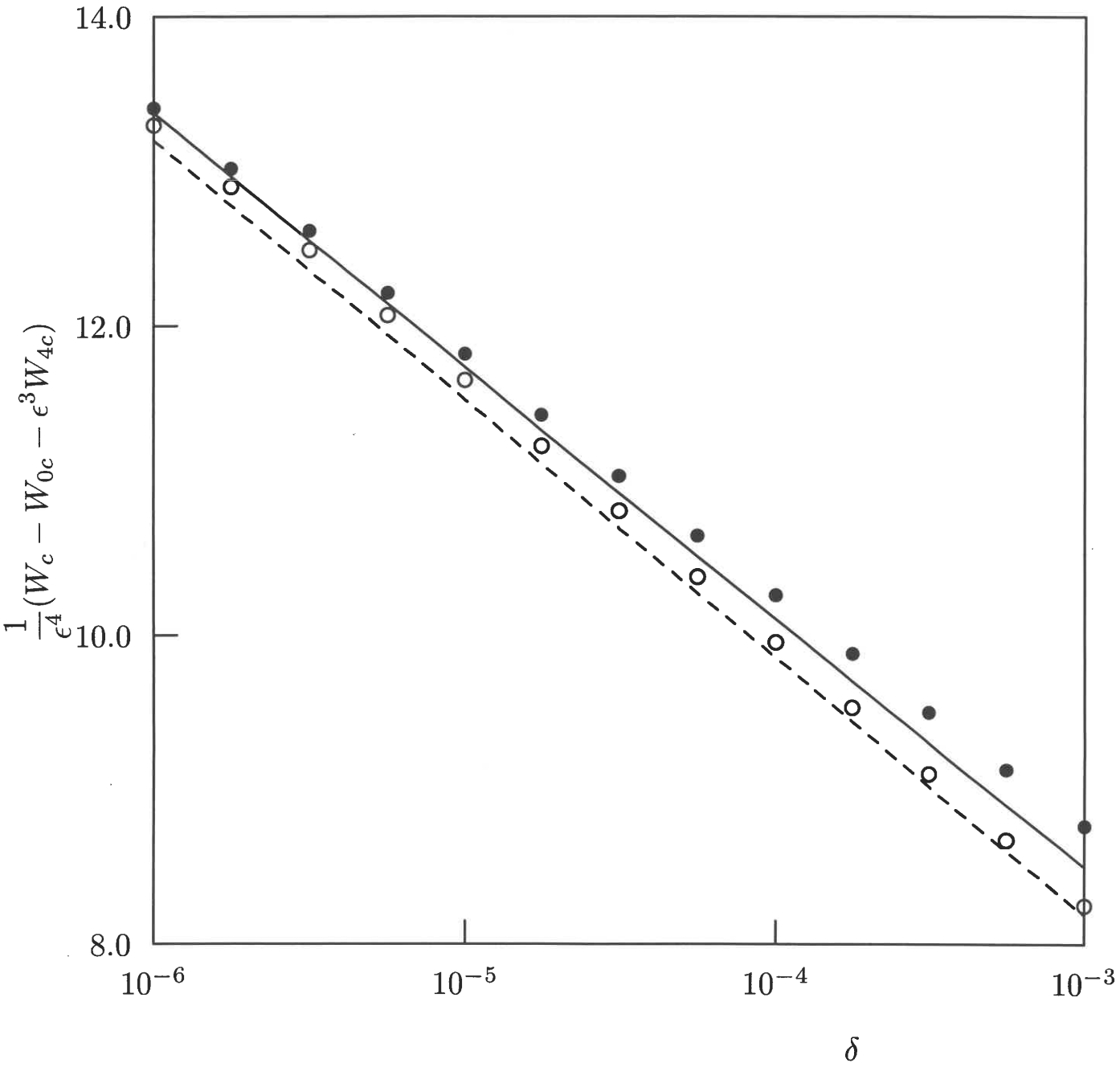
14.0
12.0
10.0
8.0
$\frac{1}{\epsilon^4}(W_c - W_{0c} - \epsilon^3 W_{4c})$
10^{-6}
10^{-5}
10^{-4}
10^{-3}
δ

Figure 6

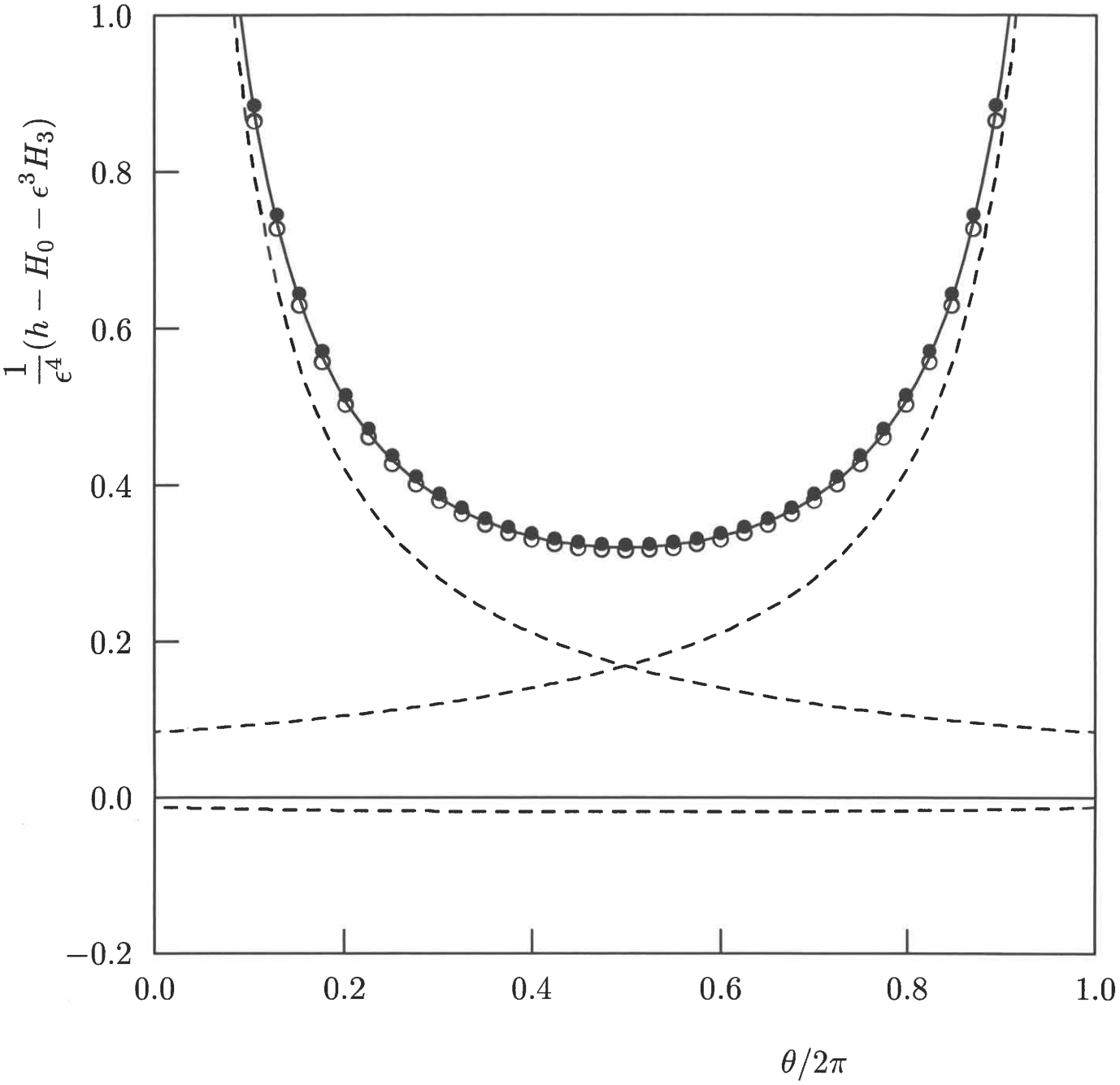
1.0
0.8
0.6
0.4
0.2
0.0
−0.2
0.0
0.2
0.4
0.6
0.8
1.0
$\frac{1}{\epsilon^4}(h - H_0 - \epsilon^3 H_3)$
$\theta/2\pi$

Figure 7(a)

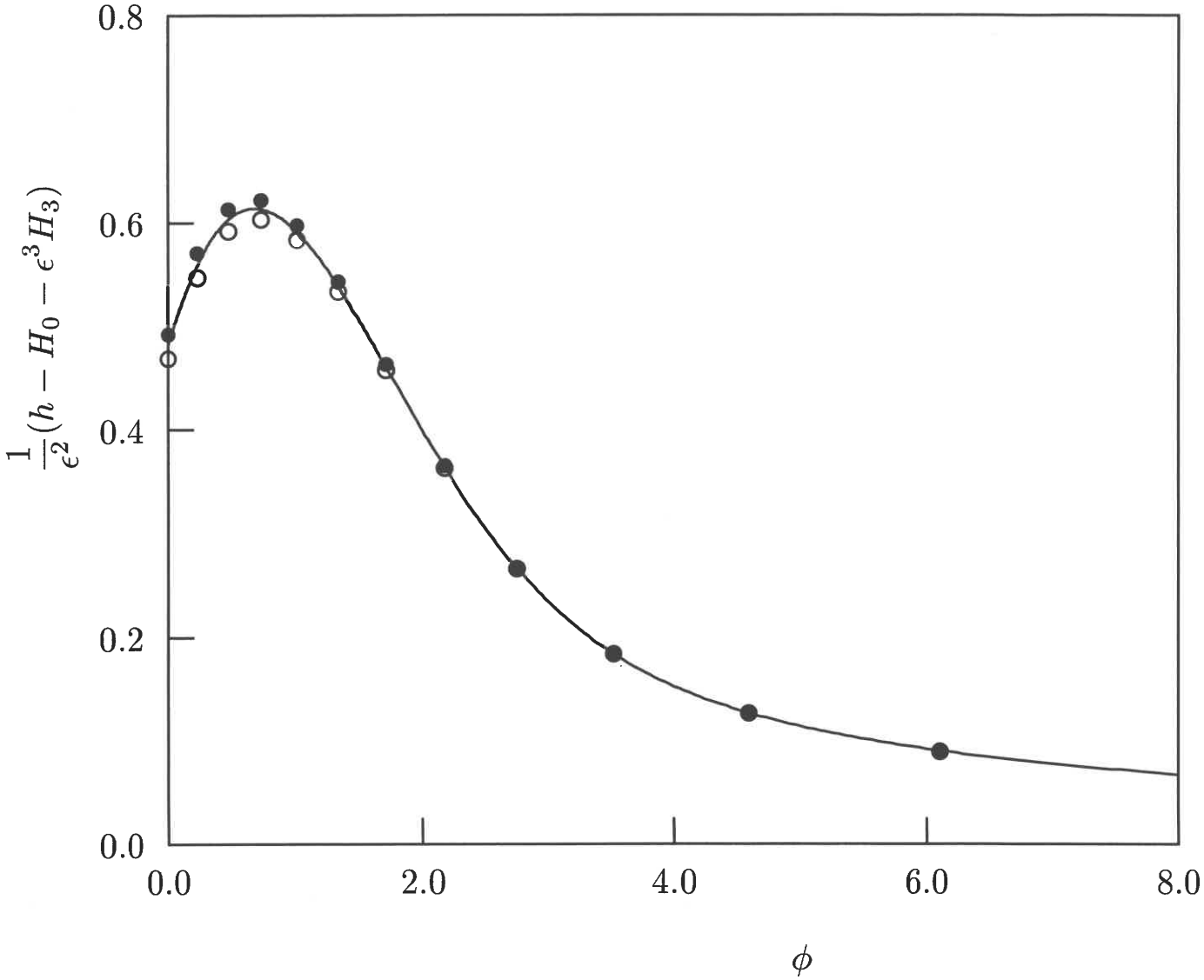

Figure 7(b)

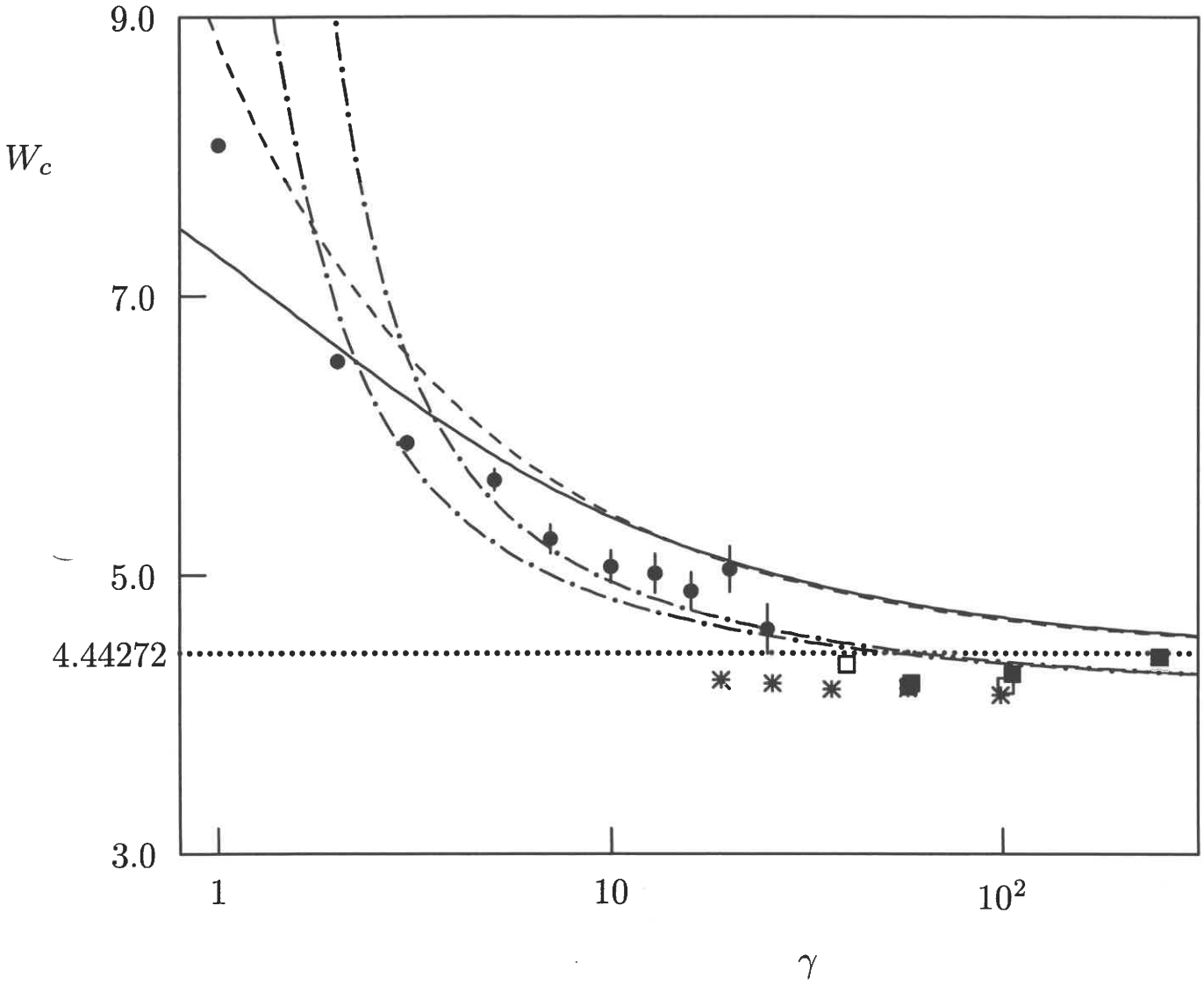

Figure 8(a)

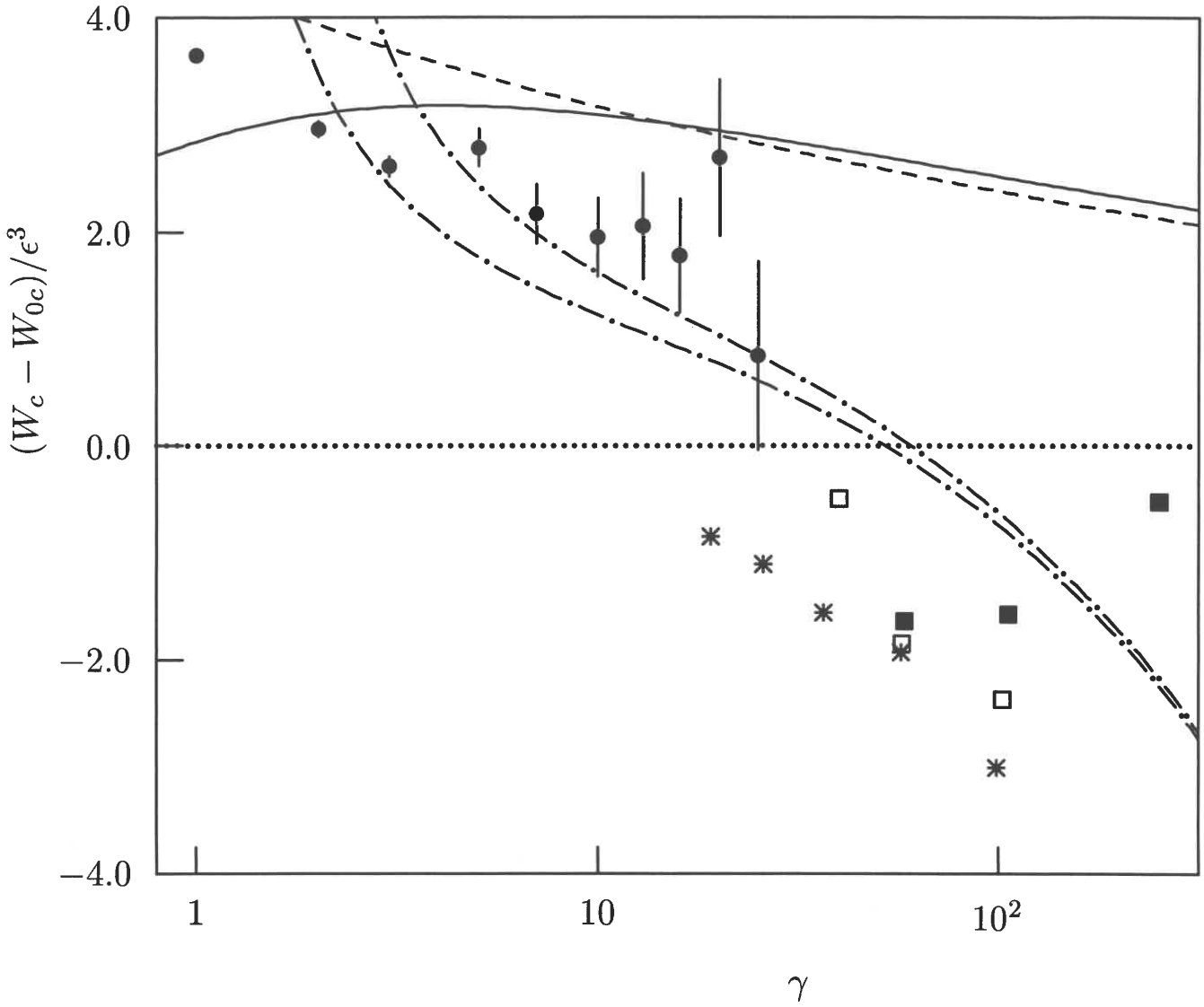

Figure 8(b)

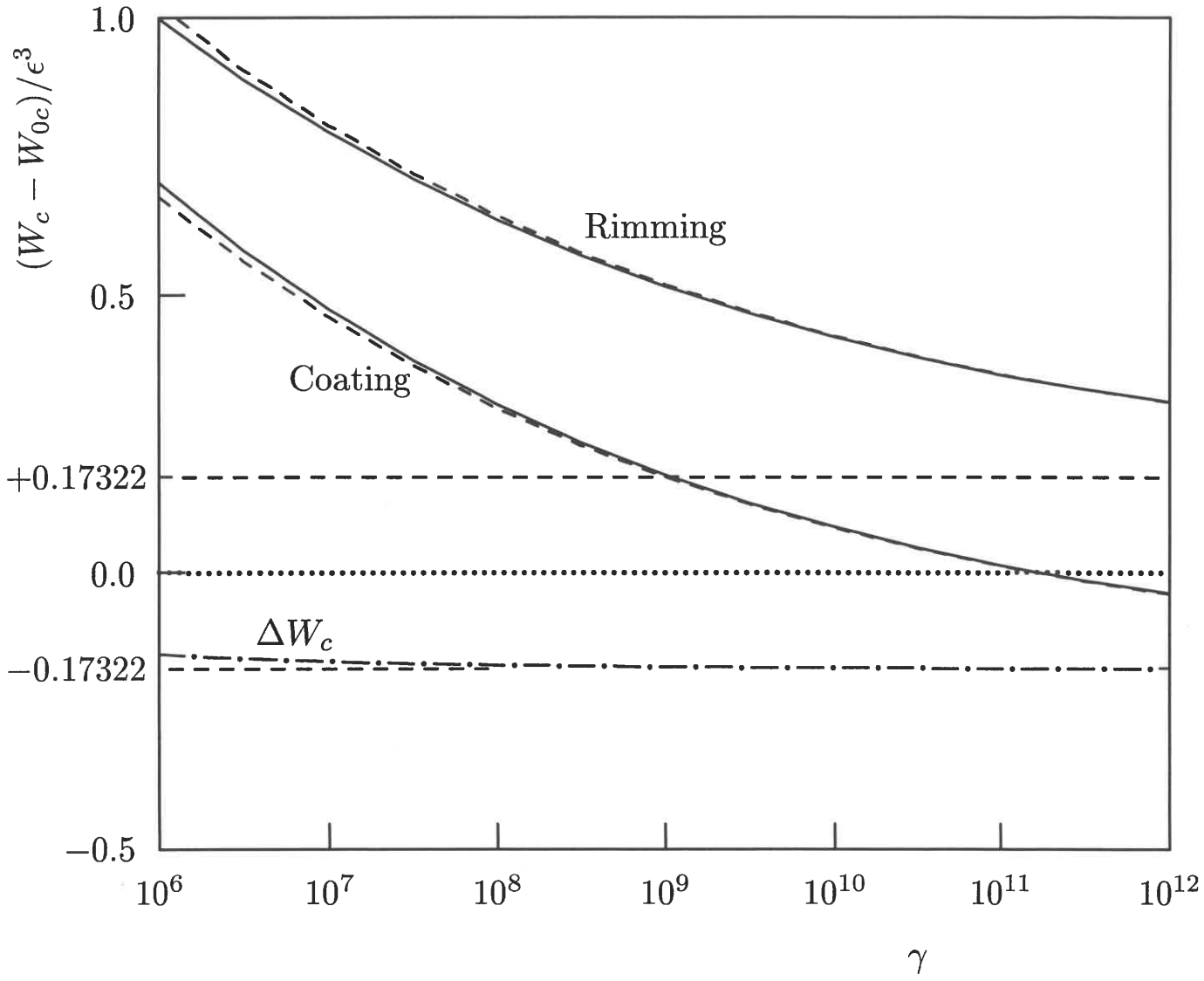
1.0
0.5
+0.17322
0.0
−0.17322
−0.5
$(W_c - W_{0c})/\epsilon^3$
Rimming
Coating
ΔW_c
10^6
10^7
10^8
10^9
10^{10}
10^{11}
10^{12}
γ

Figure 9